Science and Technology of Advanced Materials

ISSN: 1468-6996 (Print) 1878-5514 (Online) Journal homepage: www.tandfonline.com/journals/tsta20

Recent progress in Fe- and Ru-based full-Heusler bulk thermoelectrics

F. Garmroudi, M. Parzer, T. Mori & E. Bauer

To cite this article: F. Garmroudi, M. Parzer, T. Mori & E. Bauer (2025) Recent progress in Fe- and Ru-based full-Heusler bulk thermoelectrics, Science and Technology of Advanced Materials, 26:1, 2517537, DOI: 10.1080/14686996.2025.2517537

To link to this article: https://doi.org/10.1080/14686996.2025.2517537

Published online: 27 Aug 2025.

SCIENCE AND TECHNOLOGY OF ADVANCED MATERIALS
2025, VOL. 26, NO. 1, 2517537
https://doi.org/10.1080/14686996.2025.2517537

Taylor & Francis
Taylor & Francis Group

FOCUS ISSUE REVIEW

OPEN ACCESS Check for updates

Recent progress in Fe- and Ru-based full-Heusler bulk thermoelectrics

F. Garmroudi [a,b], M. Parzer[a], T. Mori [c] and E. Bauer[a]

[a]Institute of Solid State Physics, TU Wien, Wien, Austria;
[b]Materials Physics Applications - Quantum, Los Alamos National Laboratory, Los Alamos, USA;
[c]International Center for Materials Nanoarchitectonics (WPI-MANA), National Institute for Materials Science (NIMS), Tsukuba, Japan

ABSTRACT

Full-Heusler compounds represent a rich and diverse class of functional materials, covering a large compositional phase space. Representatives with 24 valence electrons are commonly semimetals or narrow-gap semiconductors as per the Slater-Pauling rule and are thus considered as thermoelectric materials, especially for room-temperature applications. Research on the archetypal thermoelectric full-Heusler compound Fe_2VAl began over two decades ago, and since then, significant progress has been made in enhancing its thermoelectric performance. Advances have been achieved through various intrinsic and extrinsic substitutions, grain boundary engineering and other optimization strategies. Here, recent advancements are reviewed, challenges for the further development of competitive full-Heusler thermoelectrics are identified, and novel routes and concepts are highlighted that could make these materials viable for energy harvesting and cooling applications near room-temperature.

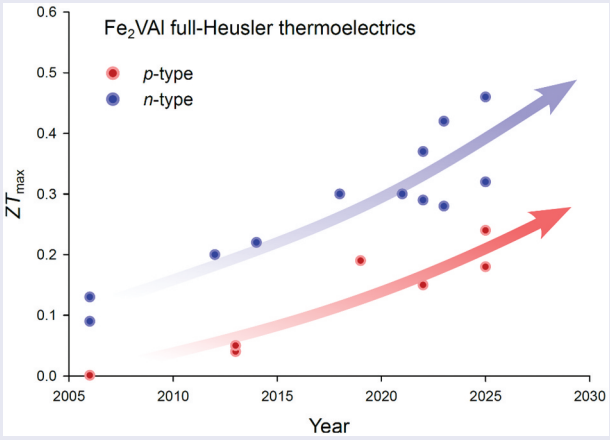

IMPACT STATEMENT

Full-Heusler compounds have emerged as important functional materials. Here, we review latest achievements for Fe- and Ru-based full-Heusler narrow-gap semiconductors as thermoelectric materials. Recent years have seen tremendous progress when it comes to enhancing the efficiency of these materials, reaching now values of the figure of merit zT up to 0.4–0.5 at room temperature. Our review will be valuable to the thermoelectric community seeking to employ new materials for near room-temperature applications.

ARTICLE HISTORY
Received 1 April 2025
Revised 19 May 2025
Accepted 4 June 2025

KEYWORDS
Full-Heusler materials; thermoelectricity; electronic and thermal transport; DFT calculations

1. Introduction

Thermoelectricity is a steadily growing field in solid-state physics, computational materials science, chemistry and various branches of engineering. It seamlessly integrates fundamental research with application-driven developments and holds great potential for energy saving and recovery across multiple domains. Industrial processes, technical devices and everyday appliances inevitably lose part of their initial energy input as waste heat, rather than fully converting it into useful mechanical, thermodynamic or electrical work.

To recover – at least – a fraction of these losses would be invaluable with respect to economy as well as ecology. Thermoelectric generators can convert such waste heat into electricity, albeit with a limited efficiency, which generally remains below 10% today. The efficiency, η, of thermoelectric devices depends on the temperature range (Carnot efficiency) and is governed by the specific active thermoelectric materials via the

CONTACT F. Garmroudi fgarmroudi@lanl.gov Institute of Solid State Physics, TU Wien, Wiedner Hauptstraße 8-10, Wien A-1040, Austria

temperature-dependent dimensionless figure of merit, ZT [1,2]. The latter combines the Seebeck coefficient S, the electrical resistivity ρ and the thermal conductivity κ – comprising the electronic (κ_{el}) and lattice contributions (κ_{ph}) – as $ZT = TS^2/(\rho\kappa)$. Typically, $ZT > 1$ is considered as a benchmark for useful applications. Since, however, the physical quantities constituting ZT are interdependent, increasing ZT is difficult, requiring sophisticated concepts and strategies.

Currently, the only materials used in commercially available thermoelectric devices and generators are alloys based on Bi_2Te_3. Known since the 1950s [3–5], these materials exhibit their highest performance at temperatures around 100 °C. While Bi_2Te_3 is, in many aspects, an almost perfect thermoelectric material, it has notable drawbacks, including limited mechanical and chemical stability, as well as concerns regarding the scarcity of Te. Addressing these limitations is crucial for developing alternative thermoelectric materials that can support broader and more sustainable applications. Criteria are, besides a reasonably large value of ZT, the availability of the respective elements, the price and the long-term ability to supply. Additionally, workability and long-term stability of the materials under thermal gradients play a crucial role in applications. In this context, full-Heusler compounds and alloys based on Fe_2VAl are promising candidates to replace Bi_2Te_3 alloys in the long run.

Here, we review recent progress in the development of Fe- and Ru-based full-Heusler compounds and outline strategies on how to improve their thermoelectric figure of merit around room temperature. Compared to their widely studied half-Heusler relatives, which are considered for mid- and high-temperature waste heat recovery, full-Heusler alloys are attractive for near room-temperature applications due to their smaller band gaps and other unique band structure features as discussed in this review. This contribution to the Science and Technology of Advanced Materials topic 'Advanced Thermoelectric Materials and Devices for Energy Harvesting' is organized as follows: First, we provide an overview of the family of Heusler compounds and their crystal structures. Next, we discuss chemical design rules and electronic structure features that make Heusler compounds promising thermoelectric materials. Thereafter, we introduce Fe_2VAl as the archetypal full-Heusler thermoelectric material and identify challenges that currently limit the applicability of these systems as well as recent progress that resulted in considerable enhancement of the thermoelectric performance. Finally, we review and present an outlook on Ru-based full-Heusler compounds as potential thermoelectric materials and directions that can be explored for the discovery of new Heusler thermoelectrics.

Heusler compounds and alloys were introduced in 1905 by Friedrich Heusler [6]. He demonstrated that a combination of non-ferromagnetic elements (Cu, Mn, Al) in an alloy yields a permanent magnetic material. Early X-ray diffraction studies by Young in 1923 [7] and Harang in 1927 [8] revealed , essentially, a cubic crystal structure with either bcc or fcc habit. Otto Heusler in 1934 [9] as well as Bradley and Rodgers [10] figured out the relevant details of the nowadays accepted crystal structure (space group: Fm-3 m, No.225, lattice parameter a = 0.5935 nm). Since then, hundreds of Heusler systems have been found and studied in detail. Many of them are successfully implemented in technical applications like in the field of spintronics, or involving qualities like shape memory properties or ferromagnetism. Besides, a large variety of ground states are present in Heusler systems, including superconductivity, magnetic skyrmions, Weyl semimetals, spin glass or magnetocaloric effects, half-metallicity, giant anomalous Nernst coefficients, as well as thermoelectricity. The widespread variation of physical properties is a consequence of the electronic structure of these X_2YZ full-Heusler systems, being intimately related to the respective cubic crystal structure. Depending on the elements involved in the X_2YZ materials, a semiconducting or metallic behavior may result as a consequence of the electronic band structure in the vicinity of the Fermi energy. In fact, a simple criterion can determine whether a given Heusler system is metallic or semiconducting, i.e. the so-called valence electron count N_{VEC} (see e.g. Ref [11]). If this count is 24, full-Heusler materials are expected to exhibit a gap in the electronic density of states around the Fermi energy. If, however, $N_{VEC} \gtrless 24$, bands are crossing the Fermi energy; thus, the system should behave metallic. Hence, thermoelectric materials based on full-Heusler systems should have their best performance for $N_{VEC} \approx 24$. Examples for such materials are Fe_2VAl or Fe_2TiSi. In addition, N_{VEC} reveals information about the magnetic state of Heusler compounds. The magnitude of the resulting permanent magnetic moment m follows the famous Slater-Pauling rule [12,13] and can be obtained from $m = (N_{VEC} - 24)\mu_B/\text{f.u.}$. Although Fe_2VAl or Fe_2TiSi contain 50% iron each, neither system exhibits magnetic ordering, in agreement with the Slater-Pauling predictions. Again, if $N_{VEC} \gtrless 24$, a permanent magnetic moment should develop and long-range magnetic ordering should be present. Examples following this rule and exhibiting magnetic order are, e.g., the archetypal compound Cu_2MnAl, various Co- and Mn-based systems, such as Co_2MnAl [14], Co_2FeSi [15], Mn2VAl [16] and countless other full-Heusler materials. In fact, Co_2FeSi ($N_{VEC} = 30$) orders magnetically as high as $T_C \approx 1100$ K and

exhibits an ordered moment $m = 6\mu_B$, in perfect agreement with the Slater-Pauling rule [15]. More recently, however, examples emerged that deviate from the Slater-Pauling rule. The implications of these deviations, particularly regarding key thermoelectric properties, are discussed later in this work.

2. Crystal structures of Heusler compounds

Ideal full-Heusler compounds of the type X_2YZ are found to crystallize in the cubic structure type Cu_2MnAl with space group Fm-3 m (no. 225); 4 formula units constitute the crystalline unit cell. X and Y are transition metals or rare earth elements, and Z is typically a main group element, e.g. from groups IIIA or IVA. In general, the atomic number Z^* is larger for the X element, i.e. $Z^*_X > Z^*_Y$. Members of this family are numerous, as e.g. Co_2MnAl, Co_2TiAl, Fe_2VAl or Ru_2TiSi, just to name a few. The unit cell of the crystal structure of X_2YZ is constituted by four interpenetrating fcc sublattices; two of them are equally occupied by X atoms. The local positions of the various elements (Wyckoff positions) in the unit cell are 8c (1/4, 1/4, 1/4) for X, 4a (0, 0, 0) for Y and 4b (1/2, 1/2, 1/2) for Z. At a local view, one of the X elements, together with the Z element form a zincblende sublattice; the second X element occupies the thus formed tetrahedral sites, while the Y element is located at the octahedral holes [17]. Depending on N_{VEC}, a broad variety of ground states have been proposed theoretically and confirmed experimentally. If one of the X elements in X_2YZ is exchanged by another one, equiatomic quaternary Heusler compounds, $X'X''YZ$, are formed. Typical examples here are CoFeCrAs, CoMnVAs, CoFeCrZ (Z = Si, As, Sb) and CoFeCrX (X = Si, Ge) [18–20]. There are several examples of so-called inverse full-Heusler compounds, where $Z^*_X < Z^*_Y$. Examples of this specific subgroup are e.g. Fe_2RhSi, Mn_2FeSi, Mn_2CoSn or Fe_2RuGe. Inverse Heusler structures are formed by interchanging the X and Y positions, which, however, reveals a different type of crystal structure. Since X is more positive than Y, a rocksalt structure is created. X atoms are placed on the Wyckoff positions 4a (0, 0, 0) and 4d (3/4, 3/4, 3/4), Y elements at 4b (1/2, 1/2, 1/2), and Z elements are found at 4c (1/4, 1/4, 1/4). The prototype of this structure is $CuHg_2Ti$, space group F-43 m (no. 216). Another subgroup of full-Heusler compounds are anti-full-Heusler systems Z_2XY, like Ga_2MnCo, Ga_2MnPd, Al_2MnCo or Al_2MnPd [21–24]. If one of the sublattices in X_2YZ is left free, half-Heusler compounds, XYZ, are originated, crystallizing in a non-centrosymmetric cubic structure (space group no. 216, F43m). The X and the Z elements are forming a zincblende structure, where the octahedral lattice sites are filled up by the Y elements. The Wyckoff positions of X, Y and Z are 4a (0, 0, 0), 4b (1/2, 1/2, 1/2) and 4c (1/4, 1/4, 1/4), respectively [17]. Typical members are, e.g., (Ti,Zr)NiSn, NbRhSn or (Nb,Ta)FeSb. These ternary half-Heusler compounds are the basis for high-performance thermoelectric materials with $ZT > 1$.

Besides the dominating cubic crystal structure of Heusler compounds, lattice distortions can lead to tetragonal Heusler systems, which are found frequently in XMn_2Z systems. Faleev et al. [25] proposed that such tetragonal distortions are originated by the peak-and-valley character of the density of states (DOS) of these compounds in the cubic phase, in conjunction with a smooth shift of the peaky DOS structure relative to the Fermi energy, when valence electrons are added to the system. Some of the Heusler compounds undergo martensitic phase transitions towards monoclinic or tetragonal phases. Examples in this respect are e.g. $Co_2Ti_{1-x}Fe_xAs$ [26] or Ni_2MnGa, exhibiting a phase transition from a cubic to a tetragonal system around 200 K [27]. Another variant of Heusler compounds exhibits a hexagonal crystal structure, space group $P6_3/mmc$, no. 194, with the prototypic Ni_3Sn structure. A typical member here is Fe_2MnGe; there, both Fe and Mn occupy the 6 h site (0.1667, 0.3333, 0.25) with occupations 2/3 and 1/3, respectively. Ge is located in the unit cell at 2c (0.3333, 0.6667, 0.25) [28]. More specific details regarding crystal structure features of the various groups and sub-groups of Heusler systems have been summarized in detail in recent review articles, e.g. in the seminal paper of Graf et al. [17] as well as in Refs [25,29,30].

A sketch of the different crystal structures is presented in Figure 1. There, the X atoms are displayed in light orange, the Y atoms in light green and the Z atoms in light blue. As was shown in detail for Fe_2VAl by DFT calculations in terms of the so-called Bader approach, there is a distinct charge transfer of 0.75 electronic charges to each Fe atom from Al (1.03) and V (0.48) [31]. Thus, bonds are drawn throughout Figure 1(a) from the X element towards the Z element. At this point, we also note that charge transfer and the lack thereof for certain defects gives rise to the existence of ionized states in Fe_2VAl; hence, very distinct scattering processes can happen [32], modifying temperature dependencies of physical properties, which are normally dictated by the scattering of charge carriers off acoustic phonons or uncharged impurities. Heusler compounds, specifically full-Heusler systems, are prone to anti-site occupations, i.e. the various constituent elements do not occupy their distinct sites, rather, atoms of a specific type interchange their local sites with other ones on another site. For instance, atoms on the 4a and 4b site frequently exchange their position, thus creating disorder on both sublattices. The probability for such transpositions depends on the formation enthalpy of such a process as

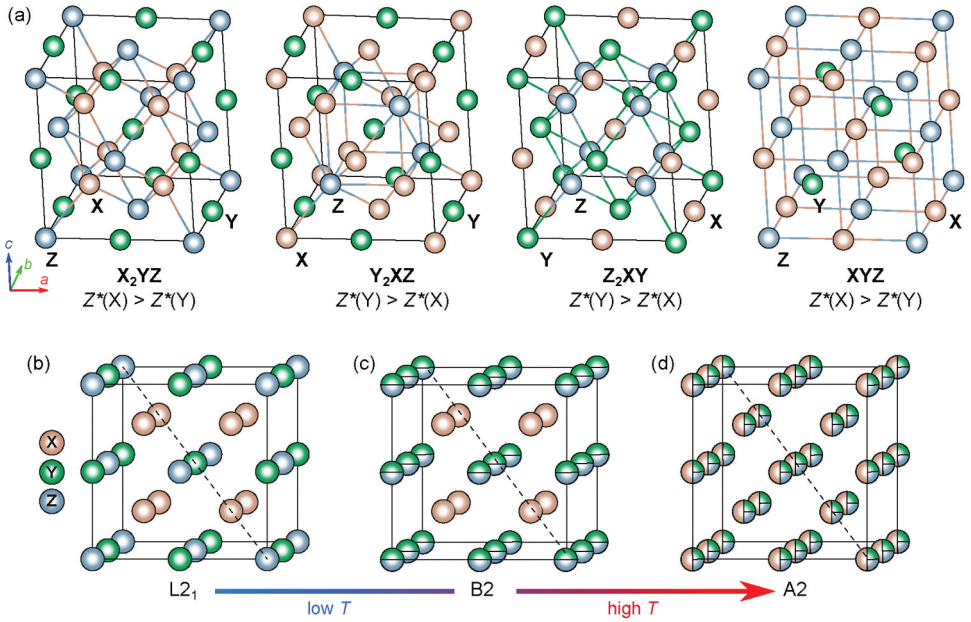

Figure 1. (a) Crystal structures for various phases of Heusler compounds; from left to right: full-Heusler compound X_2YZ, inverse-Heusler compound Y_2XZ, anti-Heusler compound Z_2XY and half-Heusler compound XYZ. Temperature- or mechanically induced order–disorder transitions frequently occur in the family of Heusler compounds and can change the crystal symmetry, e.g. from the (b) face-centered cubic $L2_1$ structure to the body-centered cubic (c) partly disorder B2 and (d) fully disordered A2 structure.

well as on the gain in configurational entropy. The latter increases linearly with temperature, which makes antisite disorder more favorable and likely at elevated temperatures, as discussed below. Employing DFT calculations, Bandaru and Jund [33] have derived formation enthalpies of different defects in Fe_2VAl, finding that the most likely transpositions are antisite defects like Al_V, Al_{Fe} and V_{Al}, significantly more energetically favorable than defects such as vacancies or interstitials. Antisite effects not only cause an increase of crystallographic disorder or modifications in the electronic density of states, but they can also entirely change the magnetic state, and a non-magnetic material can become magnetic. This was demonstrated both theoretically [33] and experimentally [34,35] on Fe_2VAl. Long-range magnetic order is established in Fe_2VAl for V vacancies as well as Fe_V and V_{Fe} antisite defects. By quenching Fe_2VAl from different heating temperatures, various states of disorder can be frozen, and physical properties can be measured straightforwardly. As a result, different overall magnetic moments have been obtained, as a consequence of the different forms of vacancies or antisite transpositions and *p*-type conduction switches to *n*-type [36]. These frozen structures mirror structural phase transitions of Fe_2VAl from A2 (at 1190 °C) to B2 (at 1080 °C) and $L2_1$ down to room temperatures [37]. The increase of disorder due to a growing number of antisite occupations, as it occurs in the thermoelectric full-Heusler material Fe_2VAl, is sketched in Figure 1(b–d). While the thoroughly ordered full-Heusler system exhibits the classical Heusler structure $L2_1$ (Cu_2MnAl-type, space group Fm-3 m, no. 225), the B2 structure (space group: Pm-3 m, no. 221) is characterized by anti-site occupations of Al and V. If eventually all elements interchange their original positions, the A2-type (space group: Im-3 m, no. 229) is approached, characterized by a fully disordered body-centered cubic structure.

3. Selecting promising thermoelectric materials from full-Heuslers

Since thermoelectric generators are thermodynamic machines, they are following Carnot's principles, i.e. the temperature range of operation is of primary importance for the thermoelectric performance of a certain thermoelectric device. Accordingly, the largest average ZT values of a distinct material need to be inside that temperature range. An initial designing principle follows $E_g \approx 10 k_B T_{work}$, where E_g is the band gap in the electronic density of states at the Fermi energy, k_B is the Boltzmann constant and T_{work} is the relevant temperature of device operation. Because the intention of the present review is focused on well performing materials in the 100 °C range, the relevant gap in the DOS of typical materials should be a few hundred meV. Several full-Heusler X_2YZ materials can be conceived, matching this criterion, either by an already existing gap of suitable width or by appropriate isoelectronic or non-isoelectronic substitutions on the various lattice sites of the X_2YZ crystalline unit cell. Heavier isoelectronic elements are expected to increase the gap in the electronic density of states, while aliovalent substitution elements shift

the position of the Fermi energy in an otherwise unchanged density of states (rigid band model). Ternary full-Heusler compounds with 24 valence electrons, like Fe_2VAl, Fe_2VGa, Fe_2TiSi, Fe_2TiSn, Ru_2NbGa, Ru_2TaAl, Ru_2TiSi, Ru_2TiGe, etc., are found to exhibit such relatively narrow gaps in the DOS near the Fermi energy. In addition, they display low-dimensional Fermi surface features owing to non-parabolic bands that are flat in certain directions of the first Brillouin zone but highly dispersive in others, creating a strongly energy-dependent transport distribution function $\Sigma(E)$, which can be derived from Boltzmann transport theory and, in the isotropic case, is formally defined as

$$\Sigma(E) = \sum_{i=1}^{N} \frac{1}{(2\pi)^3} \int \tau_{i,\mathbf{k}} v_{i,\mathbf{k}} v_{i,\mathbf{k}} \delta(E - E_{i,\mathbf{k}}) d^3\mathbf{k}, \quad (1)$$

simplifying for spherical Fermi surfaces to $\Sigma(E) = D(E)v^2(E)\tau(E)$. $D(E)$, $v^2(E)$ and $\tau(E)$ are the electronic density of states, the squared group velocity of charge carriers and the energy-dependent carrier relaxation time, respectively. $\Sigma(E)$ determines all electronic transport properties of a material, including the power factor

$$\sigma S^2 = \frac{\left[\int_{-\infty}^{\infty} \Sigma(E) \frac{E-\mu}{T} \left(\frac{-\partial f_0(E)}{\partial E}\right) dE\right]^2}{\int_{-\infty}^{\infty} \Sigma(E) \left(\frac{-\partial f_0(E)}{\partial E}\right) dE}, \quad (2)$$

where σ is the electrical conductivity, S the Seebeck coefficient, μ the chemical potential and f_0 the Fermi-Dirac distribution function. As originally pointed out by Mahan and Sofo [38], well performing thermoelectric materials should exhibit a strong energy dependence of $\Sigma(E)$, the ideal form of which would be a delta-distribution function $\Sigma(E) \sim \delta(E - E_0)$, with μ situated a few $k_B T$ away from E_0. This can be achieved by (i) a distribution of charge carrier energies as narrow as possible and (ii) high carrier velocities in the direction of the applied electric field [39], which requires, for the former, flat energy bands, but for the latter, strongly dispersive bands near the Fermi energy. Such bands can, in fact, be found in various full-Heusler systems, like in Fe_2VAl (see Figure 4) or Fe_2TiSi, and other isovalent Fe_2YZ-based members. There, Fe-e_g states form a very flat conduction electron band, with almost no dispersion along Γ – X but a strong dispersion in other Brillouin zone directions. As mentioned previously, simple chemical rules of electron counting, such as the Slater-Pauling rule, allow one to identify systems where E_F falls close to such a band edge. For full-Heusler compounds, semiconducting ground states are usually realized when the compound has a total of 24 valence electrons, while half-Heusler relatives require 18 valence electrons. Almost all promising thermoelectric Heusler materials are valence-balanced systems with an average valence electron count (VEC) of six valence electrons per atom.

4. The full-Heusler compound Fe_2VAl

In the realm of thermoelectrics, full-Heusler systems based on Fe_2VAl undeniably stand out as the most extensively studied members within the full-Heusler family. Subsequently, this section provides a concise overview of previous experimental and theoretical studies. Following that, a discussion is undertaken regarding the most critical research gaps that have been effectively addressed in recent years and need to be addressed further to make this material competitive to state-of-the-art Bi_2Te_3 semiconductors.

4.1. Experimental considerations

Fe_2VAl-based systems have gained considerable interest from both a fundamental point of view and also for applications such as thermoelectrics, owing to their peculiar electronic structure, which has been a subject of extensive debate. In particular, Nishino et al. already observed a semiconductor-like transport behavior over two decades ago [42]. The Arrhenius-type behavior of the electrical resistivity at high temperatures $\rho(T) \propto \exp(E_g/(2k_B T))$ suggests a finite band gap of 0.1 eV, comparable to that of the correlated narrow-gap semiconductor FeSi. Photoelectron spectroscopy measurements by Soda et al. [43], on the other hand, showed a clear Fermi cutoff, indicating a rather metallic ground state DOS. Together with a moderately enhanced effective mass derived from specific heat measurements at low temperatures, the question of whether Fe_2VAl could be a possible candidate for a 3*d* heavy fermion compound was raised by Nishino et al. in 1997 [42]. In response to these assertions, various experimental studies, including optical conductivity [44] and nuclear magnetic resonance [45,46], were carried out. These measurements falsified the previously suggested scenario and instead proposed a pseudogap of 0.2 eV or larger (compare Table 1). In this context, the density of states at the Fermi energy $D(E_F)$ remains finite but small, accounting for the semiconductor-like characteristics observed. These interpretations align with early theoretical studies by Weinert and Watson in 1998 that predicted hybridization-induced band gaps in various transition metal aluminides, including Fe_2VAl [47]. Moreover, the 3*d* heavy fermion scenario was further excluded by field-dependent specific heat measurements, performed by Lue et al. in 1999 [61], who instead invoked strong spin fluctuations as the primary cause for the enhanced effective masses, inferred from heat capacity measurements [42].

Table 1. Energy band gap E_g for stoichiometric Fe_2VAl from the literature [31,32,42,44,45,47,48–53], derived by various *ab initio* methods [54–59] and experiments. Large negative and positive values of E_g are possible, depending on the treatment of exchange correlation effects which are used for the band structure calculations.

	Method	Band gap	Reference
DFT:	LDA (FLASTO)	−0.2 eV	Weinert, Watson [47]
	LSDA, LAPW	−0.2 eV	Singh, Mazin [48]
	PBEsol	−0.2 eV	Shastri et al. [49]
	SCAN	−0.16 eV	Shastri et al. [49]
	GGA-PBE	−0.1 eV	Bandaru et al. [53]
	GGA-EV	−0.06 eV	Do et al. [52]
	GGA+U_{Fe-d}	−0.0092 eV	Hinterleitner et al. [31]
	QSGW	0.21 eV	Tomzcak [159]
	mBJ	0.22 eV	Shastri et al. [49]
	B1WC$_{a=0.16}$ eV	0.34 eV	Bilc et al. [50]
	GGA + $U_{Fe-d,V-d}$	0.55 eV	Do et al. [52]
	PBE0	0.58 eV	Do et al. [52]
	B1WC$_{a=0.25}$	0.62 eV	Do et al. [52]
	HSE06	1.2 eV	Lee et al. [60]
Experiment:	Seebeck & resistivity	−0.12 eV	Garmroudi et al. [32]
	Seebeck coefficient	0.002 eV	Hinterleitner et al. [31]
	Seebeck coefficient	0.02 − 0.04 eV	Anand et al. [51]
	Seebeck coefficient	0.002 eV	Hinterleitner et al. [31]
	Electrical resistivity	0.1 eV	Nishino et al. [42]
	Photoconductivity	0.1 − 0.2 eV	Okamura et al. [44]
	NMR Knight shift	0.22 eV	Lue et al. [45]
	Spin relaxation rate	0.27 eV	Lue et al. [45]

From a perspective of thermoelectric measurements, the Seebeck coefficient reaches sizable values up to 70μV K^{-1} in the undoped material [31] and even larger absolute values up to 180μV K^{-1} in *n*-doped and 110μV K^{-1} in *p*-doped samples [62] with a peak close to room temperature, indicative of narrow-gap semiconductors [31,63–65]. Indeed, when modeling the temperature-dependent Seebeck coefficient from 4 to 800 K within a parabolic two- or three-band framework, a tiny positive band gap $\approx$ 2 meV is obtained for the undoped compound (see Figure 2(a)). Furthermore, Anand et al. modeled the carrier-concentration dependence of the Seebeck coefficient for various Fe_2VAl-based samples with aliovalent substitution (see Figure 2(b)) and found an optimal band gap around $E_g = 0.02$ eV to describe the data. These fitted values, however, depend on the scattering parameter, which is initially assumed/set when modeling temperature-dependent transport

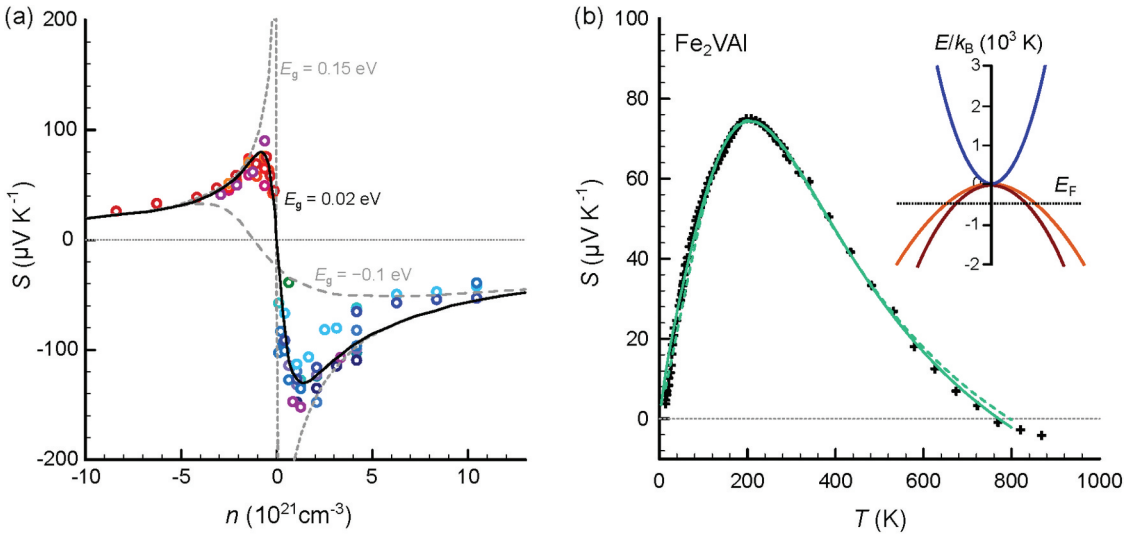

Figure 2. (a) Seebeck coefficient of Fe_2VAl-based compounds as a function of the carrier concentration for various aliovalent substitution studies [63,64,66–78]. Solid, dashed and dotted lines are model results, employing a parabolic two-band model with dominant acoustic phonon scattering. Different values of the band gap E_g are compared. While a negative band overlap (semimetal) $E_g = -0.1$ eV fails to describe the experimental data, the data can be well described assuming a finite band gap of $E_g = 0.02$ eV. Data are taken from ref [51]. (b) Temperature-dependent Seebeck coefficient of Fe_2VAl. Solid and dashed lines represent least-squares fits to the experimental data, employing a triple and two-parabolic band model, respectively. The resulting band structure (inset) features a tiny positive band gap $\approx$ 2 meV between valence and conduction bands and an almost degenerate set of valence bands, consistent with density functional theory calculations employing GGA + *U* functionals.

properties. Therefore, fitting results can give varying values in the range −0.15 eV up to +0.002 eV, depending on the choice of relevant model parameters [32].

4.2. Theoretical considerations

Figure 3(a) shows the density of states of Fe_2VAl with the respective atom-decomposed partial densities of states. It can be seen that Fe states give the largest contribution to the overall DOS, whereas Al has a minimal contribution in the energy range −6 to 3 eV. Vanadium has a sizable contribution to the DOS above the Fermi energy as the conduction band dangling into the pseudogap (*X* band) has mainly V e_g orbital character. Standard density functional theory (DFT) calculations in the local density approximation (LDA) or general gradient approximation (GGA) reveal a large negative indirect band overlap at different high-symmetry points in the reciprocal space (−0.2 to −0.1 eV) [47–49,79]. Simple exchange correlation functionals, such as LDA- and GGA-type functionals, thus cannot explain the semiconductor-like transport behavior and large Seebeck coefficients found experimentally. Considering hybrid functionals with different admixture parameters or enhanced correlation effects in terms of an effective onsite Coulomb repulsion, the band gap can be increased drastically from −0.2 up to 1.2 eV with a large variance of possible values in between, depending on the chosen functional (see Table 1). It was shown that corrections to the DFT calculations in terms of the single-particle Green's function and screened Coulomb interaction (GW corrections) can lead to more consistent results among the different functionals [60]. Hinterleitner et al. investigated the effect of introducing an effective on-site Coulomb repulsion among Fe *d* orbitals $U_{\text{eff}} = U - J$, where *U* is the Coulomb repulsion and *J* the exchange interaction. A large number of U_{eff} values were screened, and the temperature-dependent electronic transport properties (Seebeck coefficient, electrical resistivity) were calculated from the resulting band structures in the constant relaxation time approximation. By comparing their theoretical results to experimental data, a recommended value of $U_{\text{eff}} = 2.145$ eV for the Fe *d* orbitals was determined by the authors, resulting in a tiny negative band overlap $E_g = E_X - E_\Gamma = -0.009$ eV when calculating the band structure using this set of parameters. Figure 3 (b) compares the band structure of Fe_2VAl for different values of the on-site Coulomb repulsion term taken into account for the Fe-*d* orbitals. It can be seen that the band gap expands as the Fe e_g states are pushed towards higher energies, whereas Fe-dominated t_{2g} states are pushed towards lower energies. Interestingly, even the V-e_g conduction states at X are affected and slightly raised in energy.

Bilc and Ghosez [50], Venkatesh et al. [80] as well as Bandaru and Jund [33] have pointed out that antisite defects can result in significant

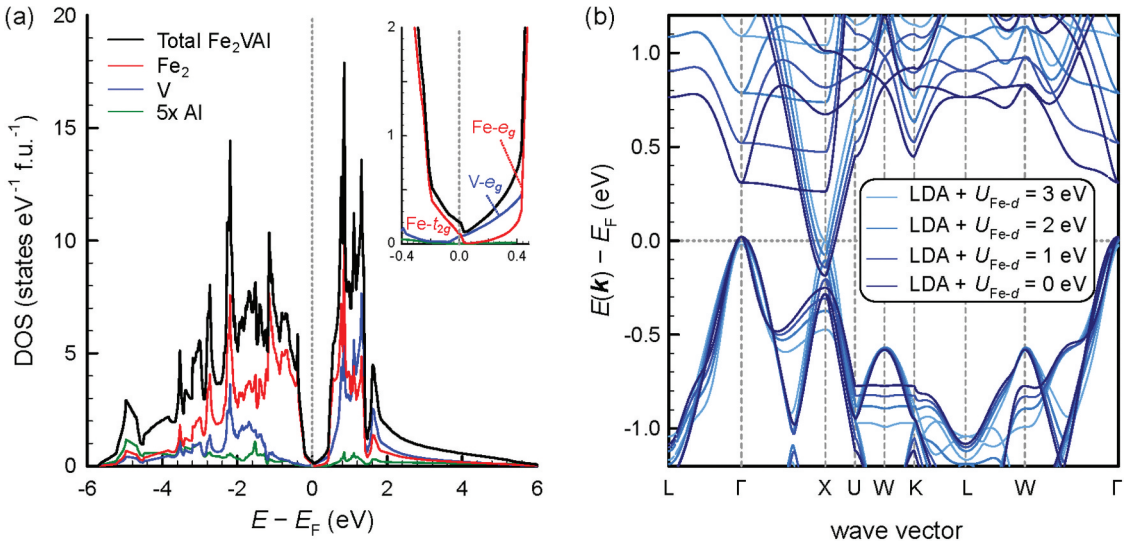

Figure 3. (a) Calculated (GGA-PBE) electronic density of states (DOS) of Fe_2VAl with atom-decomposed contributions. Inset shows a close-up of the DOS around E_F, relevant for electronic transport. It can be seen that the valence band consists mostly of Fe t_{2g} states while the conduction band crossing E_F has mainly V e_g orbital character. The rather localized states ≈ 0.4 eV above E_F originate from Fe e_g orbitals. (b) and (c) shows the band structure of Fe2VAl considering additional on-site Coulomb repulsion for Fe *d* orbitals and V *d* orbitals in the DFT calculations (LDA + *U*). An opening of the gap is apparent, driven by the Coulomb repulsion among Fe or V *d* states. (d) Temperature-dependent Seebeck coefficient of Fe_2VAl. Black crosses are experimental data; solid and dashed lines are theoretical predictions, calculated from the band structure in the constant relaxation time approximation.

modifications of the electronic structure. Without knowing the exact contribution from defects and their local interactions in real samples, it has not been possible to derive a precise assessment of the intrinsic electronic structure so far. The same holds true for electronic correlation effects which are set as additional input parameters and hardly calculable ab initio. Recently, claims such as a temperature-induced band gap increase stemming from thermal expansion and thermally activated V/Al inversion defects have been invoked by Berche et al. [81] in order to justify the disparity between metallic low-temperature photoemission spectroscopy data and semiconductor-like high-temperature transport properties. These results, however, are based upon the assumption that V/Al inversion defects form clusters around Fe atoms. To this end, it is important to highlight that the authors overlooked the fact that, at elevated temperatures, a considerable increase in the configurational entropy term contributes significantly to the Gibbs enthalpy, favoring a disordered arrangement of defects and decreasing the likelihood of an ordered cluster configuration.

Summarizing, there have been ample theoretical attempts to explain experimental observations: (i) A semimetallic band structure with a vanishingly small band overlap [31] (ii) a wide-gap band structure with impurity in-gap states induced by antisite disorder [50], (iii) a semimetallic band structure with a temperature-induced band gap opening due to thermal expansion and antisite defects [81], as well as more exotic interpretations such as (iv) a metallic band structure incorporating dynamical correlation effects [82]. To conclude this section, it is crucial to emphasize that engaging in a meaningful discussion and theoretical comparison with experimental results of nominally stoichiometric Fe_2VAl is futile without accounting for inevitable antisite defects and their critical role in altering electronic and magnetic properties in manifold aspects.

5. Challenges and progress in Fe_2VAl thermoelectrics

5.1. Narrow band gap and bipolar conduction

As discussed in the previous section, although there is still ambiguity with respect to the precise value of the band gap, the full-Heusler compound Fe_2VAl has typically been reported to feature an almost zero-gap or even semimetallic band structure with a small overlap of its valence and conduction bands. Still, the Seebeck coefficient can nonetheless reach sizable values in this system due to highly asymmetrical band features and a quasi-low-dimensional Fermi surface. Kato et al. first demonstrated that introducing Si at the Al site in $Fe_2VAl_{1-x}Si_x$ effectively adjusts the charge carrier concentration and induces a rigid-band-like shift of E_F, already yielding substantial power factors $PF \approx 5.5\,\mathrm{mW\ m^{-1}\ K^{-2}}$ [66], larger than those of Bi_2Te_3 systems and most other state-of-the-art semiconductors, while also maintaining large Seebeck coefficients up to $120-130\,\mathrm{m}VK^{-1}$. Subsequent investigations revealed even higher power factors, reaching up to $6.7\,\mathrm{mW\ m^{-1}\ K^{-2}}$ [62] and $6.8\,\mathrm{mW\ m^{-1}\ K^{-2}}$ [83] in off-stoichiometric variations, such as $Fe_{2-x}V_{1+x}Al_{1-y}Si_y$ and $Fe_2V_{1+x}Al_{1-x}$. Therefore, it is not surprising that over the course of the last years the primary focus of research has been on reducing the lattice thermal conductivity of Fe_2VAl. However, to achieve substantial enhancements of the figure of merit ZT, it is crucial to further tune the band structure via band engineering as well, especially considering the rather low values of the Seebeck coefficients in p-type Fe_2VAl-based full-Heuslers, which hinders progress in enhancing ZT. Indeed, even in the metallic limit, that is, if lattice-driven heat transport could be minimized such that heat transport is entirely dominated by electrons $\kappa_{el} \gg \kappa_{ph}$, the limit $ZT \approx S^2/L$ – L being the Lorenz number – indicates that for p-type compounds, with S generally of the order of $100\mu\mathrm{V\ K^{-1}}$ or less, it is impossible to obtain ZT values that are competitive with Bi_2Te_3 and its alloys with Sb_2Te_3. Anand et al. pointed out that an enhancement of the band gap is crucial to further optimize the TE performance of Fe_2VAl-based thermoelectrics [51]. Certainly, an enhancement of the band gap increases the quality factor $\tilde{B} = (k_B/e^2)(\sigma_{E0}/\kappa_{ph})E_g$ in materials – σ_{E0} being the electronic quality factor – where two bands actively contribute to TE transport [84]. Increasing E_g not only allows for larger values of the Seebeck coefficient to be realized but also reduces bipolar thermal conductivity, whose contribution is significant in Fe_2VAl-based systems at $T > 300\,\mathrm{K}$.

5.1.1. V site substitutions to expand band gap

Since the pseudogap states dangling into the band gap and overlapping in energy are dominated by Fe-t_{2g} states for the valence band (VB) and V-e_g states for the conduction band (CB), rational substitutions at the Fe or V sublattices are crucial to expand the band gap. What has proven as an effective way of expanding the band gap and thereby increasing the Seebeck coefficient and overall performance are co-substitutions on the V sublattice [40,41]. Figure 4 compares the band structure near the Fermi level of the isovalent full-Heusler compounds Fe_2VAl, Fe_2TaAl and Fe_2TiSi, obtained in terms of standard GGA-PBE exchange correlation functionals. While Fe_2VAl displays

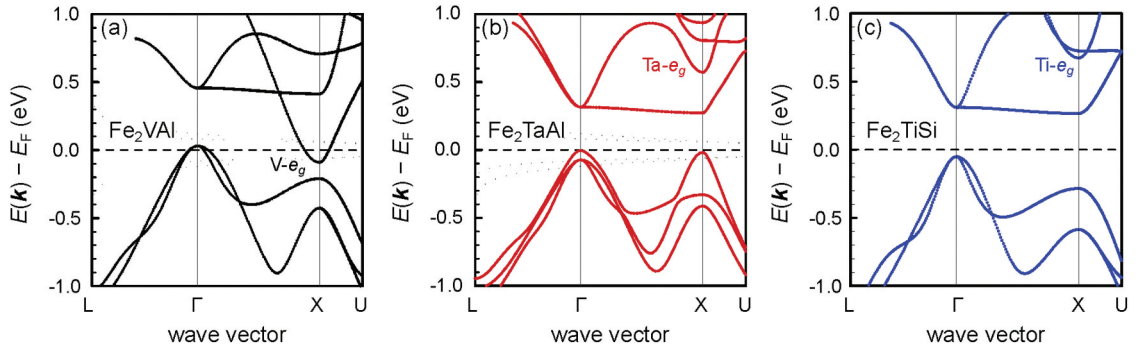

Figure 4. Electronic band structures at equilibrium volumes obtained from DFT calculations using GGA-PBE-type exchange correlation functionals. (a) Fe_2VAl, (b) Fe_2TaAl (with spin – orbit coupling). (c) Fe_2TiSi. While Fe_2VAl is a semimetal the latter two are semiconductors due to Ta- and Ti-e_g states being higher in energy. Computational data were obtained by the authors in previous studies [40,41] and computational details are summarized in the respective references.

a semimetallic band structure, the other two compounds are predicted to be semiconductors, as the Y site-dominated e_g conduction bands are pushed towards higher energies. In the case of Fe_2TaAl, one may assume that this results from the 5*d* states of Ta being located higher in energy than the 3*d* states of V. For Fe_2TiSi, the lower nuclear atomic charge and reduced Coulomb attraction likely explain the higher lying e_g orbitals in this compound and the resulting semiconducting ground state.

An interesting and crucial question is, whether a continuous band gap opening can be achieved by partial substitution, especially since the stoichiometric compounds Fe_2TaAl and Fe_2TiSi are metastable and have so far not been successfully synthesized as single-phase materials in bulk form. Figure 5 shows the evolution of the electronic structure of Fe_2VAl-based Heusler compounds upon partial substitution of V with Ti and Ta. Since Ti has one less valence electron than V, it is necessary to co-substitute Si at the Al site to balance the Fermi level. By a surplus of Ti doping or Si doping, the properties can be varied from *p*-type to *n*-type. Similarly, in the case of Ta substituted Heusler compounds, Ti and Si can be co-doped to enable a shift of the Fermi level further into the VB or CB. Figure 5(a) shows the unfolded electronic band structure of $Fe_2V_{1-x}Ti_xAl_{1-y}Si_y$ ($x, y \approx 0.15$), obtained from DFT supercell calculations [41] using GGA-PBE functionals with an on-site Coulomb correction (GGA + U, $U_{Fe-d} = 2.145$ eV). The white solid lines represent the band structure of stoichiometric pristine Fe_2VAl using the same computational parameters. It can be clearly seen that even for rather small substitutions x, y, an increase of the band gap is still

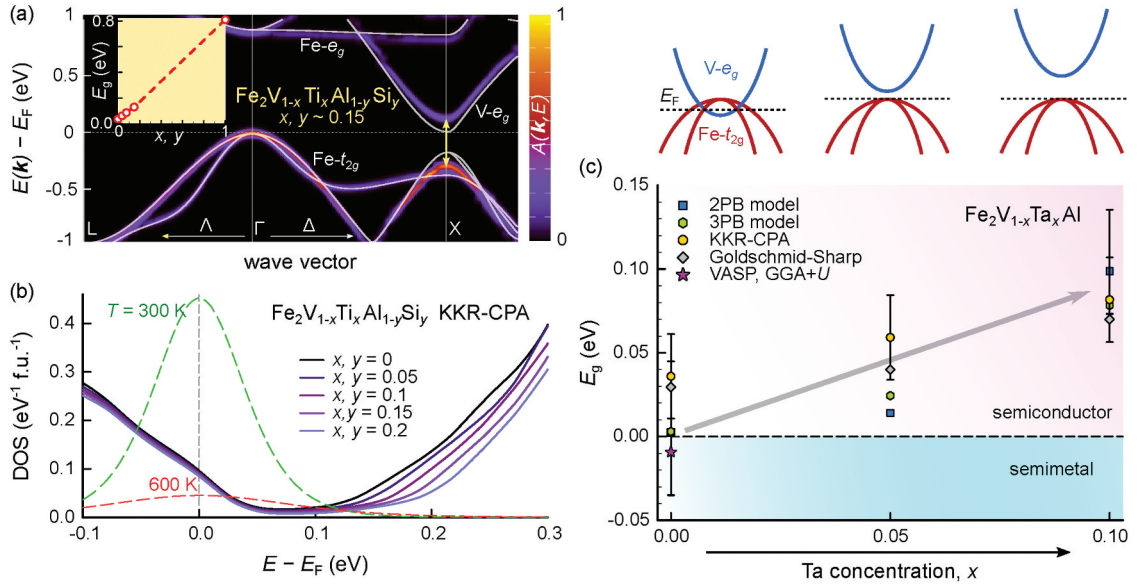

Figure 5. Band gap opening by partial Ta and Ti substitutions at the V site. (a) Unfolded band structure of partially substituted $Fe_2V_{1-x}Ti_xAl_{1-y}Si_y$ with $x = y = 0.15$. Inset shows a continues increase of the band gap with increasing x, y. (b) Alloy-averaged densities of states of $Fe_2V_{1-x}Ti_xAl_{1-y}Si_y$ for various concentrations of x, y. Green and red dashed lines show derivative of the Fermi-Dirac distribution at 300 and 600 K, respectively. (c) a continuous expansion of the band gap is also confirmed for partial Ta substitution in $Fe_2V_{1-x}Ta_xAl$. Computational data and figures were reproduced from Refs [40,41].

visible as the V-e_g-dominated band is shifted towards higher energies. The inset in Figure 5(a) highlights that there exists a continuous, almost linear increase of the band gap between the two Heusler compounds (Fe_2VAl and Fe_2TiSi). Consistent and qualitatively similar results are also found for DFT-based calculations using the framework of the Kohn-Korringa-Rostoker method and the coherent potential approximation (KKR-CPA), which accurately capture alloy disorder arising from the random substitution of Ti and Si atoms at the V and Al sublattices, respectively (see Figure 5(b)). The same picture holds true and has been confirmed experimentally also for partial Ta substitution in $Fe_2V_{1-x}Ta_xAl$ (see Figure 5(c)). Thus, it is possible to tune (expand) the band gap of Fe_2VAl via partial substitution of Ta and Ti at the V site. As shown in Figure 6(a), this leads to significantly higher Seebeck coefficients, $S > 190\,\mu V\ K^{-1}$, which can be realized in these co-substituted systems. Consequently, ultrahigh values of the thermoelectric power factor, $PF > 10\,mW\ m^{-1}\ K^{-2}$ were achieved, which are more than two times larger than those of the best Bi_2Te_3-based systems (see Figure 6(b)). We note that these values constitute the record among *n*-type semiconductors, whereas even larger power factors are achieved in metallic systems with scattering-induced electron–hole asymmetry such as the intermediate valence Kondo system $YbAl_3$ [90] and binary transition metal alloys [91]. The highest power factor of any material above room temperature is obtained in binary Ni_xAu_{1-x} alloys, with $PF_{max} \approx 34\,mW\ m^{-1}\ K^{-2}$ at 560 K and an ultrahigh average $PF_{av} \approx 30\,mW\ m^{-1}\ K^{-2}$ in the temperature range 300–1100 K for $x = 0.1$ [91].

5.1.2. Off-stoichiometry and self-subsitution

Another approach to modify the electronic structure of Fe_2VAl is self-substitution, where the compound is doped with its own constituents – Fe, V and Al. This approach offers advantages such as a high solubility limit for various substitution strategies and a straightforward synthesis process, as all three elements are inexpensive and easy to handle. Various studies on off-stoichiometry in Fe_2VAl have explored different substitution variations, including Fe/V [62,92–97], V/Al [83,98–103], Fe/Al [96,104], as well as Fe, V/Al off-stoichiometry [67,92,105–110]. Notably, full solubility from V_3Al to Fe_3Al was reported in $Fe_{2+x}V_{1-x}Al$ [111], and an exceptionally high solubility limit of $x = 0.2$ was found for Fe, V substitution with Al in $Fe_{2-2x}V_{1-x}Al_{1+3x}$ [108,110]. Additionally, no solubility limits were observed for V/Al and Fe/Al substitutions up to 20% [83,104]. For thermoelectric applications, the self-substitution of Al with V, combined with V/Ti substitution, has shown promising results, achieving the highest TE performance in *p*-type Fe_2VAl materials reported to date (ZT up to 0.24 at 400 K) [101,103,112]. This improvement can possibly be attributed to a slight band gap opening due to the off-stoichiometry and the V/Ti substitution, as described above. Following a related approach, Parzer et al. employed double-site substitution of V and Al atoms by Ti to expand the band gap, although decreasing the Al content ultimately results in a closure of the band gap following the transition from Fe_2VAl to Fe_2Ti_2 [113]. Thus, a sweet spot exists, where E_g and consequently S can be enhanced, leading to $ZT \approx 0.2$.

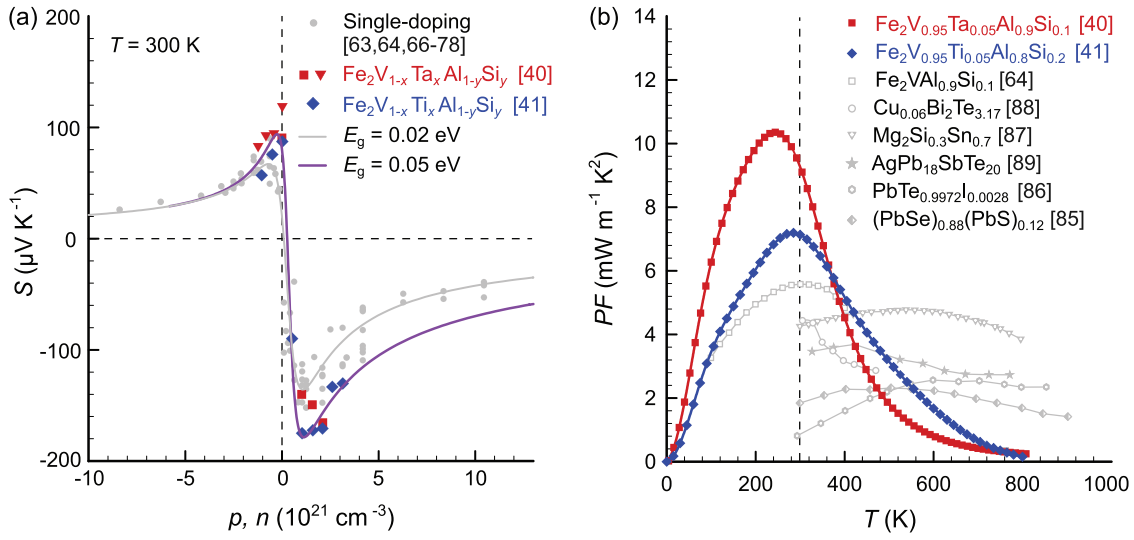

Figure 6. Thermoelectric performance enhancement by band gap engineering. (a) Pisarenko-style plot of room-temperature Seebeck coefficient versus chemical carrier doping concentration of single-doped Fe_2VAl-based Heusler compounds [63,64,66–78] and co-substituted systems [40,41] based on $Fe_2V_{1-x}Ta_xAl_{1-y}Si_y$ and $Fe_2V_{1-x}Ti_xAl_{1-y}Si_y$, (b) temperature-dependent power factor of optimally doped co-substituted Heusler compounds with an enhanced band gap versus single-doped $Fe_2VAl_{0.9}Si_{0.1}$ [64] and other state-of-the-art *n*-type thermoelectric materials [85–89].

On the other hand, the simultaneous substitution of Fe and V with Al was found to induce more drastic changes in the electronic structure [108,110]. As highlighted in Figure 7(a,b) Al self-substitution leads to a significant flattening of the Fe-dominated valence band together with a substantial band gap opening reaching close to $E_g = 0.3$ eV in $Fe_{1.78}V_{0.89}Al_{1.33}$. This was traced back to a lack of *d-d* hybridization of the Al antisites with the surrounding V and Fe atoms. Consequently, the Seebeck coefficient is nearly doubled compared to stoichiometric Fe_2VAl and its maximum shifts towards higher temperatures close to 400 K, as bipolar conduction is reduced (see Figure 7 (c)). Figure 7(d,e) show the composition-dependent change in the Seebeck coefficient and the band gap E_g, extracted from $S(T)$ via the three-band model [114] and from DFT supercell band structure calculations, analyzing multiple samples along the $Fe_{2-2x}V_{1-x}Al_{1+3x}$ series for $x = 0 - 0.2$ [110]. A continuous trend is observed with increasing Al substitution: up to 11% substitution of Fe and V atoms with Al, the band gap increases, while for higher x, it decreases. Interestingly, this band gap opening occurs despite substantially increasing disorder within the system and can be understood as a hybridization gap, as discussed in more detail in Refs [47,110]. Moreover, the similarity between $S(x)$ and $E_g(x)$ underscores the importance of reducing the bipolar conduction, for instance, through band gap opening in Fe_2VAl. Finally, the increased disorder leads to a reduced thermal conductivity in off-stoichiometric compounds, most drastically in the case of $Fe_{2-2x}V_{1-x}Al_{1+3x}$ [108].

Besides introducing self-substitution/antisite defects through off-stoichiometry, Fe_2VAl Heusler compounds have the unique ability to promote the formation of antisite defects even in their stoichiometric, pristine form upon changing the heat treatment. As discussed previously and highlighted in Figure 1(b–d), Fe_2VAl undergoes two structural order–disorder transitions at high temperatures. First, at around 1080 °C, the fully ordered $L2_1$ structure transforms into the partly disordered B2 phase (CsCl-type), where the V and Al sublattices become disordered, that is, Al and V atoms can exchange and mix on the respective 4a and 4b Wyckoff positions. Then, at 1190 °C, a further transformation into the

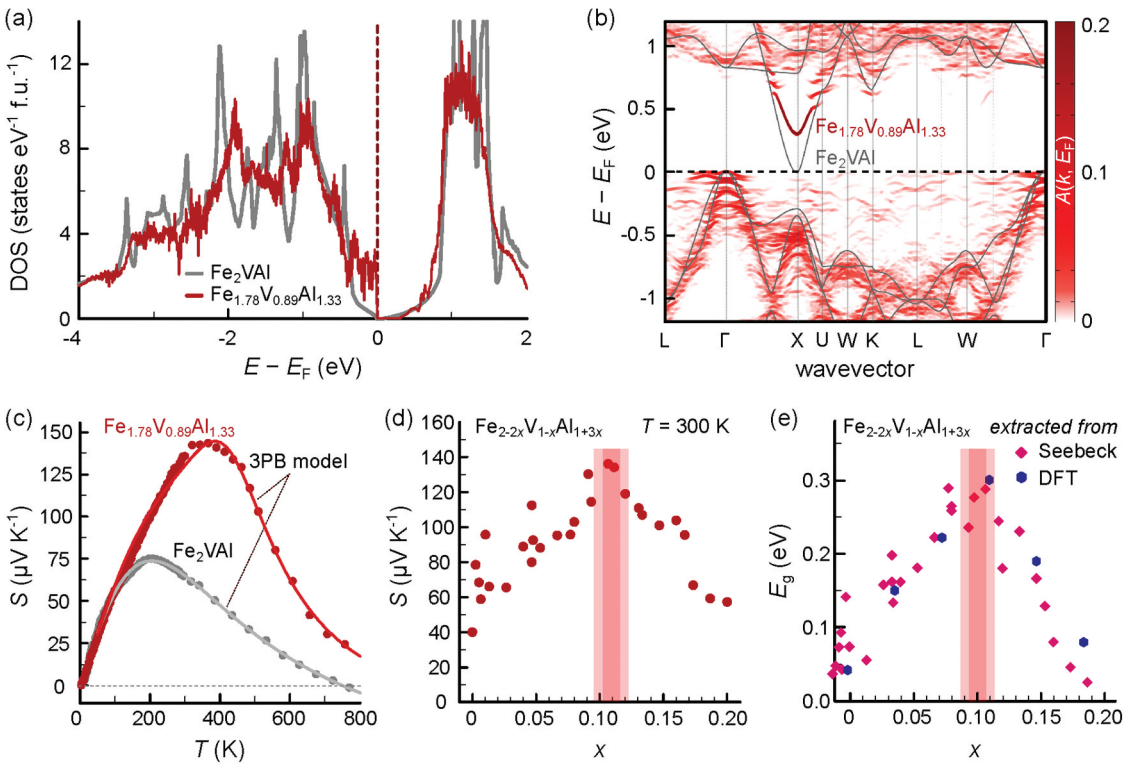

Figure 7. (a) Comparison of the densities of states of stoichiometric Fe_2VAl with the Al-rich $Fe_{1.78}V_{0.89}Al_{1.33}$ compound. (b) Comparison of the band structures of stoichiometric Fe_2VAl with the Al-rich $Fe_{1.78}V_{0.89}Al_{1.33}$ compound. For the off-stoichiometric calculation, a 108-atomic supercell was calculated, subsequently employing band unfolding. (c) Comparison of the temperature-dependent Seebeck coefficient of the two compounds. Clearly, the Al-substitution leads to a significant increase in $S(T)$. (d) Seebeck coefficient at room temperature for multiple samples along the $Fe_{2-2x}V_{1-x}Al_{1+3x}$ stoichiometry ranging from $x = 0 - 0.2$. The red area highlights the samples that are close to the theoretical highlighted compound in panels (a-c), with $x = 0.11$. (e) Extracted band gap for the same samples from both, temperature dependence of the experimental Seebeck coefficients (red diamonds), and DFT calculations (blue hexagons). The Seebeck coefficient follows a similar trend as the band gap, confirming the strong correlation between E_g and $S(T)$ in these compounds. Experimental and computational data were obtained by the authors in a previous study [110].

fully disordered A2 structure (W-type) takes place. Maier et al. used in-situ neutron diffraction at high temperatures to investigate the structural transitions [115], and Garmroudi et al. modelled the order–disorder transitions using Monte Carlo simulations based on effective cluster interactions and statistical thermodynamics [34,116]. Moreover, in the Refs [34,116], it could be shown that the antisite defects present at high temperatures can be (partially) frozen by thermal quenching. Antisite defects involving the Fe sublattice lead to the formation of localized magnetic impurity states within or near the pseudogap of the compound. Thereby, the degree of antisite disorder can be directly correlated with the magnetic properties and even estimated from the saturation magnetization at low temperatures. At low concentrations, impurity states associated with these defects are localized due to Anderson and Mott localization and therefore do not contribute directly to thermoelectric transport. When increasing the concentration of defects, a quantum percolation threshold is reached, where electrons become delocalized in the center of the impurity band. This Anderson transition switches the conduction-type from *p*-type to *n*-type as charge carriers from the impurity states eventually outweigh holes from the valence band states in stoichiometric Fe_2VAl [34]. Crucially, even though the system turns more metallic, the Seebeck coefficient increases and remains large as electronic states are stacked in a narrow energy interval, which enhances the density-of-states effective mass. This way, large values of the power factor up to 4 mW m^{-1} K^{-2} [35] and 7.6 mW m^{-1} K^{-2} [34] could be achieved in stoichiometric Fe_2VAl via thermal treatment.

It is interesting to note that for stoichiometric Fe_2VAl it is not possible to stabilize the fully disordered A2 phase by thermal quenching [34,107], whereas in Si-substituted $Fe_2VAl_{0.9}Si_{0.1}$, the entire A2 structure can indeed be obtained experimentally in bulk samples, which was explained by a change in the diffusion kinetics of defects upon substituting Si for Al [116]. The A2 phase displays a ferromagnetic and fully metallic ground state, as demonstrated theoretically and experimentally [116,117]. Thus, an intermediate number of antisite defects is likely optimal for thermoelectric performance, although achieving reproducible samples and properties might be challenging, given the fact that ordering and diffusion kinetics during quenching change depending on the exact composition.

5.2. Inhibiting lattice-driven heat transport

Inarguably, the major bottleneck hindering the realization of high *ZT* values in Fe_2VAl-based compounds is the intrinsically high lattice thermal conductivity of this compound. Depending on the exact synthesis conditions and the defects introduced thereby, κ_{ph} usually ranges between 15 and 30 W m^{-1} K^{-1} at 300 K, which is at least an order of magnitude higher than that of optimized Bi_2Te_3-based materials. Since heat carried by the lattice does not contribute to the conversion of thermal energy into electrical power, it reduces the efficiency of thermoelectric conversion processes and needs to be suppressed as much as possible. Owing to the high intrinsic κ_{ph} in Fe_2VAl, provoked by very high values of the sound velocity, the primary focus of research has been on reducing κ_{ph} via various strategies. Below, we review some of the most promising conceptions that effectively reduced κ_{ph}, and discuss ongoing challenges that need to be overcome to further boost *ZT*.

5.2.1. Heavy-element substitution

One of the most effective methods to reduce κ_{ph} in thermoelectric materials is alloying elements with large volume or mass differences. The associated strain and mass fluctuations will scatter high-frequency heat-carrying phonons. Figure 8 displays the combined efforts of several research groups to reduce κ_{ph} by extrinsic (co) substitution with foreign atoms [64,67,68,118–122] as well as by self-substitution via off-stoichiometric sample preparation [83,96]. The full-Heusler crystal structure with similar fcc sublattices and a vast phase space of elemental compositions allows substitution at all lattice sites, offering a huge playground for tuning functional properties. Since bipolar conduction plays a significant role at room temperature, κ_{ph} extracted from the total measured κ subtracted by the electronic part, which is estimated by the Wiedemann-Franz law, still contains the bipolar term, i.e. $\kappa - \kappa_{el} = \kappa_{ph} + \kappa_{bi}$. Table 1(a, b) summarize the absolute values of $\kappa_{ph} + \kappa_{bi}$ and the relative reduction of $\kappa_{ph} + \kappa_{bi}$ with respect to pristine Fe_2VAl as a function of the concentration of the substituted elements for different single-site substitution studies. It can be seen that substitutions with heavy 5*d* elements, such as Ta [121,125] and W [67,68] at the V site or Re [118] and Ir [120] at the Fe site, lead to the lowest values of $\kappa_{ph} + \kappa_{bi}$ with the exception of $Fe_2VAl_{1-x}Ta_x$. However, it was shown that, in this case, Ta preferentially occupies the V positions, and V atoms are pushed towards the Al site as antisite defects [121].

By co-substituting multiple elements at different lattice sites (see Figure 8(c,d)), $\kappa_{ph} + \kappa_{bi}$ can even be further reduced down to 2–3 W m^{-1} K^{-1} in $Fe_{1.95}W_{0.05}V_{0.98}Ta_{0.1}Al_{0.92}$, which reaches a record-high $ZT > 0.3$ for substituted Fe_2VAl-based systems without grain refinement. As shown in Figure 9, the tradeoff between lattice thermal conductivity and carrier mobility, as a major challenge in further enhancing *ZT* by substitution in Fe_2VAl-based full-Heuslers, is identified. This is particularly true for *n*-type materials, where 5*d* elements are substituted at the V site. As previously established, the conduction band of

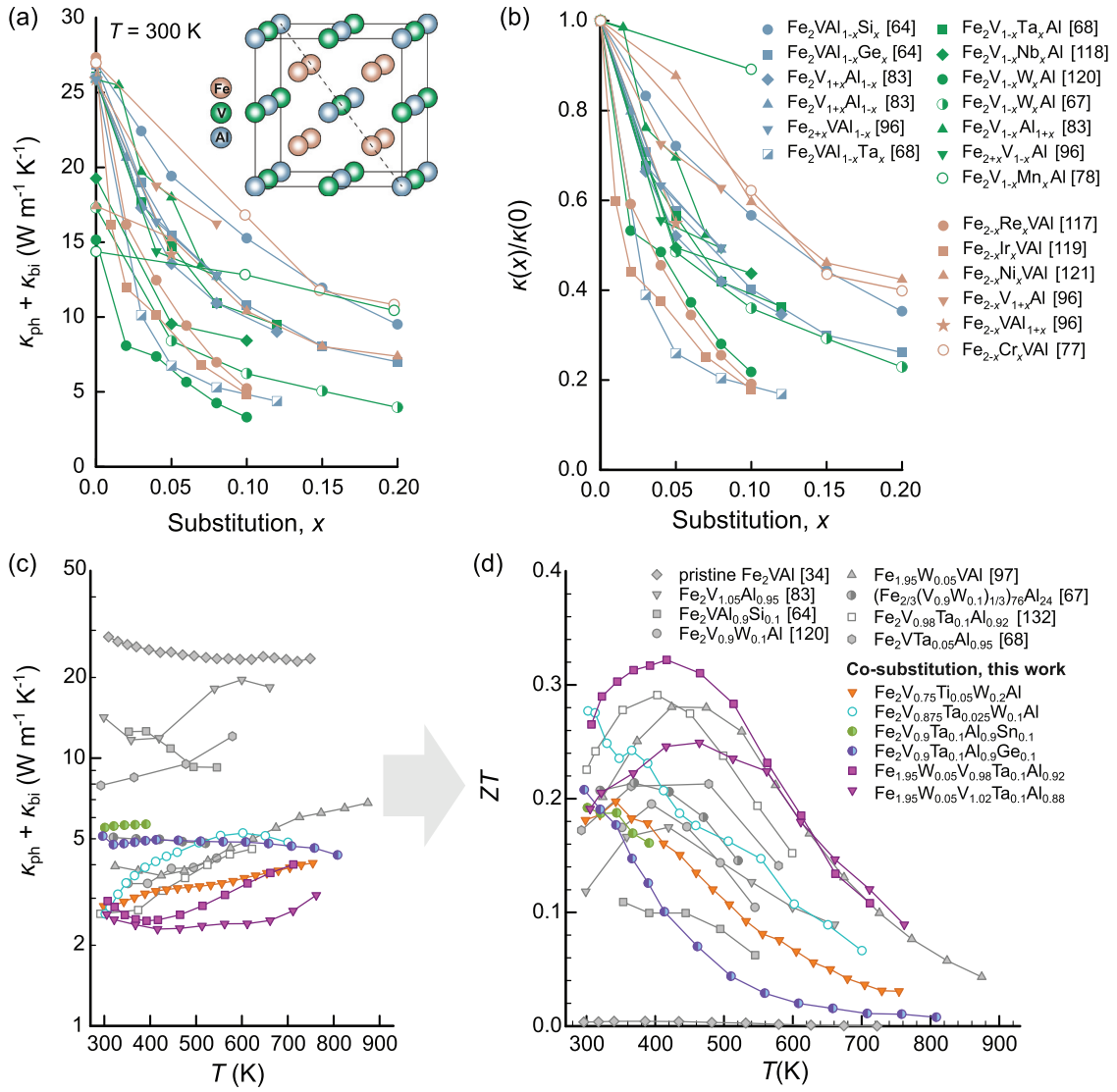

Figure 8. Reduction of lattice thermal conductivity by various substitutions [34,64,67,83,96,97,120,123,124] in Fe_2VAl-based full-Heuslers. (a) Composition-dependent room-temperature lattice thermal conductivity plus bipolar contribution ($\kappa_{ph} + \kappa_{bi}$) of Fe_2VAl-based systems with single-site substitution at Fe, V and Al sites. (b) Relative reduction of $\kappa_{ph} + \kappa_{bi}$ in (a) compared to the value of the stoichiometric compound reported in the respective literature study. (c) Temperature-dependent $\kappa_{ph} + \kappa_{bi}$ for different single-substituted and co-substituted and co-substituted Fe_2VAl-based Heusler thermoelectrics. (d) Temperature-dependent *ZT* corresponding to the materials shown in (c). A record-high maximum $ZT \approx 0.34$ among all substituted systems is found for $Fe_{1.95}W_{0.05}V_{1.02}Ta_{0.1}Al_{0.92}$ with substitution at all lattice sites. Gray symbols in (c) and (d) refer to data taken from the literature and colored symbols represent data collected for samples synthesized for the first time in this work. All materials were synthesized via induction melting as described in ref [40].

Fe_2VAl and related Heusler compounds has predominantly e_g orbital character attributable to the atoms at the Y site. Thus, introducing disorder at the Y site by alloying results in strong random potential fluctuations that heavily scatter charge carriers, deteriorating carrier mobility. One possible way to overcome this would be substituting heavy 5*d* elements at the Fe site (instead of the V site) and pushing the Fermi level towards the optimal position by Si or Ge substitution at the Al site. As of now, there are no reports on co-substitution studies investigating, e.g. Re or Os substitution at the Fe site, in combination with Si or Ge substitution at the Al site.

5.2.2. *Grain boundary engineering*

There have been various attempts to refine the grain structure of Fe_2VAl-based thermoelectrics, e.g. via ball milling [130,131] or high-pressure torsion (HPT) [123,132]. These techniques can decrease the grain size down to the nanoscale and induce lattice defects such as dislocations. Grain boundaries and dislocations scatter heat-carrying phonons of different wave lengths than those affected by point defects. They are, therefore, especially promising in conjunction with heavy-element substitution to scatter the whole phonon spectrum and optimally inhibit lattice-driven heat transport. Mikami et al. undertook efforts to

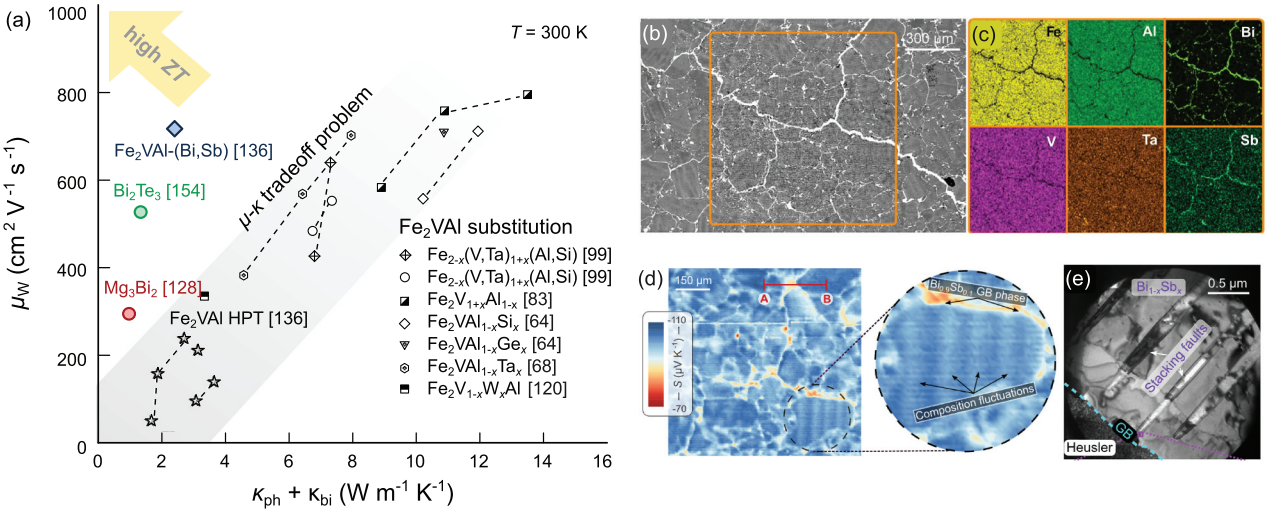

Figure 9. (a) Tradeoff between charge carrier mobility and lattice thermal conductivity. Weighted mobilities calculated using the equation presented in ref [126]. are plotted versus $\kappa_{ph} + \kappa_{bi}$ for various Fe_2VAl-based systems, where lattice-driven heat transport is inhibited by substitution [64,68,83,99,121] or grain refinement [127] state-of-the-art Bi_2Te_3 [128] and Mg_3Bi_2 [129] semiconductors are also shown for comparison. Effective strategies that aim to boost *ZT* of Fe_2VAl full-Heusler thermoelectrics have to overcome the μ-κ tradeoff problem. A promising strategy might be engineering appropriate grain boundary phases that allow for a decoupling of charge and heat transport [127]. (b) Backscattered electron microscopy images and (c) corresponding energy-dispersive x-ray mapping of the microstructure of Fe_2VAl-(BiSb) composite with decoupled charge and heat transport shown in (a). (d) Transient potential Seebeck microprobe imaging reveals a complex microstructure with composition fluctuations of the Heusler phase inside the grains and Bi-Sb grain boundary networks. (e) Bright-field transmission electron microscopy reveals arrays of stacking fault defects within the Bi-Sb grain boundary phases. Images were represented from ref [127].

synthesize various substituted Fe_2VAl-based Heusler alloys via mechanical alloying in a planetary ball mill, followed by consecutive spark plasma sintering of the fine-grained powder [68,130,131]. The powder after ball milling usually consists of micrometric particles, which are agglomerates of even smaller nanocrystallites $d \approx 20$ nm. Although grain growth occurs during the sintering process, the lattice thermal conductivity can be substantially reduced this way.

Masuda et al. [132] and Fukuta et al. [123] introduced high-pressure torsion as a technique to further reduce κ_{ph} in Fe_2VAl-based full-Heuslers. HPT utilizes high pressures of several gigapascals and torsional strain, resulting in severe plastic deformation, to introduce an abundance of local lattice defects at different length scales (micro- to nanoscale). Rogl et al. have demonstrated that HPT can boost *ZT* in skutterudites up to $ZT \approx 2$ [133–135], while only slight improvements were reported for half-Heusler compounds [136]. Employing HPT to $Fe_2V_{0.98}Ta_{0.1}Al_{0.92}$ full-Heusler compounds, Fukuta et al. recently reported record-high *ZT* values (among Fe_2VAl-based systems) up to $ZT = 0.37$ [123]. As part of a recent study, it was attempted to reproduce these results, following the same synthesis procedure; however, no enhancements of the dimensionless figure of merit were realized [127]. This indicates that setup-specific conditions and parameters during HPT are likely crucial for realizing good thermoelectric properties, complicating upscale production. Another challenge regarding grain refinement, using the techniques described above, is that full-Heusler compounds are prone to antisite disorder, even at room temperature, given that enough mechanical work is induced [107,115]. Indeed, both ball-milled and plastically deformed Fe_2VAl-based Heusler compounds commonly display a fully disordered A2 phase (see Figure 1(d)) instead of the $L2_1$ Heusler structure. This phase has a magnetic and metallic ground state [116,117]. Thus, additional annealing at high temperatures is required to recover the desired Heusler phase, which inevitably results in grain growth, and consequently an increase of the thermal conductivity, compared to the nanostructured samples without annealing [123]. In addition, the tradeoff with respect to carrier mobility (Figure 9) further hinders enhancements of *ZT*.

In a recent work, composites with topological-insulating Bi_1-xSb_x-based materials were shown to decouple charge and heat transport, bypassing this tradeoff [127]. In this approach, chemically and structurally distinct Bi_1-xSb_x was incorporated between Heusler grains during synthesis via liquid-phase sintering, resulting in compact composite materials with a rich and complex microstructure (cf. Figure 9(b–e)). Surprisingly, only the

thermal conductivity was reduced, while electrical transport remained excellent and the thermoelectric properties were significantly enhanced – results that go beyond effective medium theory predictions [137–139].

We summarize several important thermoelectric material parameters of optimized Fe_2VAl-based full-Heusler compounds in Table 2, namely the lattice (and bipolar) contribution to the thermal conductivity, the weighted mobility [126], an estimate of the thermal band gap via the Goldsmid-Sharp formula and the thermoelectric performance given by ZT_{max} and the average ZT in the temperature range 300–400 K, which is most important for harvesting low-grade waste heat. It can be seen that while ZT has long hovered around 0.1–0.2, combined efforts of composition tuning and microstructure engineering have now resulted in several materials with ZT well above 0.3 or even 0.4, meaning that the ZT around room temperature of Fe_2VAl-based materials is no longer an order of magnitude smaller than that of commercially used Bi_2Te_3 systems but merely a factor of 2–3.

6. Ruthenium-based full-Heuslers

6.1. Comparison of ruthenium- versus iron-based Heusler compounds

Among Fe-based full-Heusler compounds with VEC = 6, only Fe_2VAl and Fe_2VGa have been synthesized as single-phase materials. Although larger band gaps and semiconducting ground states have been predicted in other members such as Fe_2TiSi and Fe_2TiSn [140], Fe_2NbAl [141] or Fe_2TaZ (Z = Al, Ga, In) [142], these materials are either thermodynamically unstable compared to other more stable phases, in particular Fe_2Y-based Laves phases [143], or could only be realized as metastable or disordered materials, e.g. employing thin film growth [144–146]. On the other hand, Fujimoto et al. recently reported thermoelectric properties of Ru_2TiSi full-Heusler compounds. Due to the semiconducting ground state, the hitherto largest Seebeck coefficient among bulk full-Heusler systems was obtained over a broad range of temperatures [147]. In Figure 10, the electronic structures (extracted from the Materials Project database [148]) and the temperature-dependent Seebeck coefficient of Fe_2VAl [122] and Ru_2TiSi [147] are compared. DFT calculations of the density of states and band structure, shown in Figure 10(a), reveal that Ru_2TiSi displays a wider pseudogap and more dispersive VB states compared to its isovalent sibling compound Fe_2VAl. This can be interpreted as a result of increasing delocalization and bandwidth, when moving down the periodic table from 3*d* Fe towards 4*d* Ru. Indeed, the dispersion of the V/Ti-dominated conduction band at X hardly changes as opposed to the Fe/Ru-dominated valence band at Γ and X. An enlarged band gap and lower valence band effective mass, consistent with the DFT predictions, are also derived from least-squares fits of the temperature-dependent Seebeck coefficient $S(T)$ of both compounds, employing a two-parabolic band model (see Figure 10(b)) [149]. Despite a similar slope of $S(T)$ at low temperatures (implying a similar position of the Fermi level with respect to the VB edge), the maximum of $S(T)$ is shifted towards higher temperatures for Ru_2TiSi and reaches much larger absolute values. This is a clear indication of an enlarged band gap. Additionally, the tail of $S(T)$ within the bipolar regime is less sharp, signifying that valence band states are more mobile than in Fe2VAl. This becomes even more apparent for *p*-doped Ru2TiSi_1-xAl_x, as discussed in Ref [149].

6.2. Superior p-type thermoelectric performance in Ru_2TiSi semiconductors

Fujimoto et al. studied the effect of Ta doping in *n*-type Ru_2Ti_1-xTa_xSi [147]. Despite a significantly reduced lattice thermal conductivity, $ZT_{max} \approx 0.4$ in $Ru_2Ti_{0.8}Ta_{0.2}Si$, as reported by the authors, it did not exceed that of pristine Ru_2TiSi, which also reaches $ZT_{max} \approx 0.4$, suggesting that the weighted mobility of *n*-type samples is significantly smaller than for *p*-type compounds. This was confirmed in a previous study, where the temperature- and doping-dependent

Table 2. Important thermoelectric parameters for several optimized Fe_2VAl-based full-Heusler compounds: phonon thermal conductivity (including bipolar term), weighted carrier mobility, Goldsmid-Sharp band gap $E_g = 2e|S_{max}|T_{max}$, maximum ZT and average ZT in the temperature range 300–400 K.

Heusler material	κ_{ph} (W/Km)	μ_w (cm^2/Vs)	E_g (meV)	ZT_{max}, ZT_{av}
$Fe_2VAl_{0.9}Si_{0.1}$ [64]	14.7	679	39	0.09, 0.08
$Fe_2VAl_{0.9}Ge_{0.1}$ [64]	10.4	709	39	0.13, 0.12
$Fe_2V_{0.9}W_{0.1}Al$ [68]	3.4	314	44	0.20, 0.17
$Fe_2VAl_{0.5}Ta_{0.05}$ [121]	7.8	715	66	0.22, 0.20
$Fe_{1.95}W_{0.05}VAl$ [97]	4.0	651	51	0.28, 0.23
$Fe_2V_{0.98}Ta_{0.1}Al_{0.92}$ [123]	2.6	598	50	0.29, 0.27
$Fe_2VAl_{0.95}Ta_{0.05}$ HPT [132]	3.3	508	52	0.30, 0.26
Fe2V0.95Ta0.05Al0.9Si0.1 [160]	6.8	1024	49	0.30, 0.26
Fe1.95W0.05V0.98Ta0.1Al0.92	2.9	597	48	0.32, 0.30
$Fe_2V_{0.98}Ta_{0.1}Al_{0.92}$ HPT [123]	1.3	439	50	0.37, 0.33
$Fe_2V_{0.95}Ta_{0.1}Al_{0.95}$-Bi-Sb [127]	2.4	724	44	0.46, 0.40

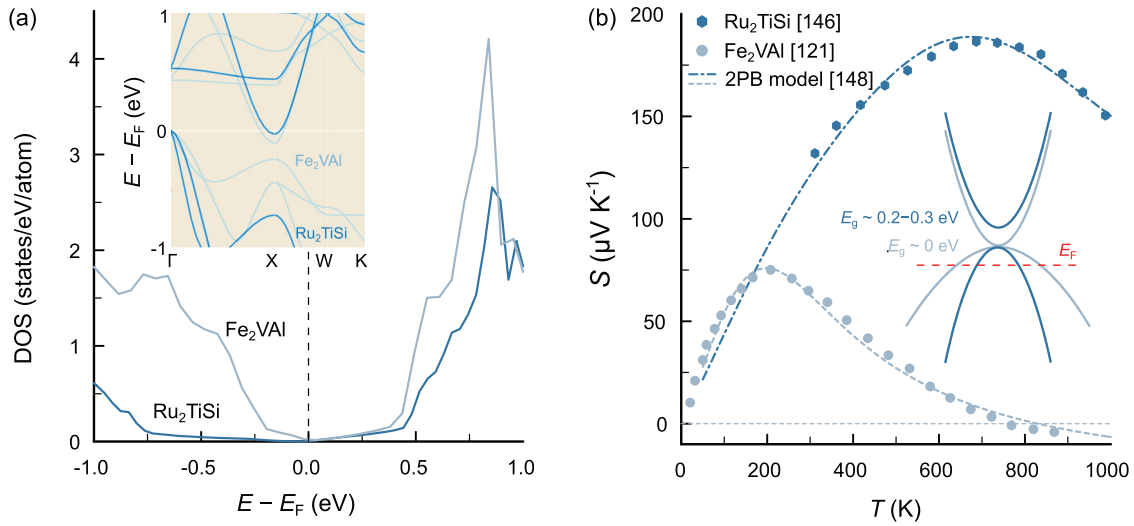

Figure 10. (a) Comparison of energy-dependent electronic density of states around the Fermi level for the stoichiometric full-Heusler compounds Fe_2VAl and Ru_2TiSi. Inset shows the band structures of both materials. More dispersive valence bands and a wider band gap is predicted for Ru_2TiSi. Computational data were extracted from the materials project data base [148] (b) temperature-dependent Seebeck coefficient of Fe_2VAl [122] Ru_2TiSi [147] dashed and dashed-dotted lines represent least-squares fits, employing a two-parabolic band model (2PB). An analysis within a 2PB model [149] predicts a wider band gap and more dispersive valence band for Ru_2TiSi, consistent with DFT calculations.

thermoelectric properties of both *p*- and *n*-type Ru_2TiSi were analyzed, revealing that the valence band electronic structure displays a far greater potential for realizing high thermoelectric performance [149]. Figure 11 summarizes the doping-dependent prediction of the thermoelectric performance – *PF* and *ZT* – of Ru_2TiSi semiconductors. For the latter, a similar reduction of κ_{ph} for different 5*d* elements substituted at the Ti site was assumed. Figure 11(b) shows that for a concentration of $x = 0.2$ in $Ru_2Ti_{1-x}Y_xSi$ (Y = hf, Ta), a ZT_{max} close to $ZT_{max} = 1$ is predicted for *p*-doped Ru_2TiSi, as opposed to a more than two times smaller $ZT_{max} < 0.5$ in *n*-type systems. These predictions motivated a study regarding the effect of Hf substitution in $Ru_2Ti_{1-x}Hf_xSi$, for which $ZT_{max} \approx 0.7$ is found when $x = 0.2$,[1] which likely can be further enhanced up to $ZT_{max} \approx 1$ by co-doping Al for Si. These results demonstrate that, next to half-Heusler compounds, full-Heusler systems also bear the potential for realizing competitive thermoelectric performance, motivating a systematic search for novel semiconducting full-Heusler phases. Here, it should be pointed out that an increasing number of theoretical studies have predicted novel full-Heusler semiconductors X_2YZ

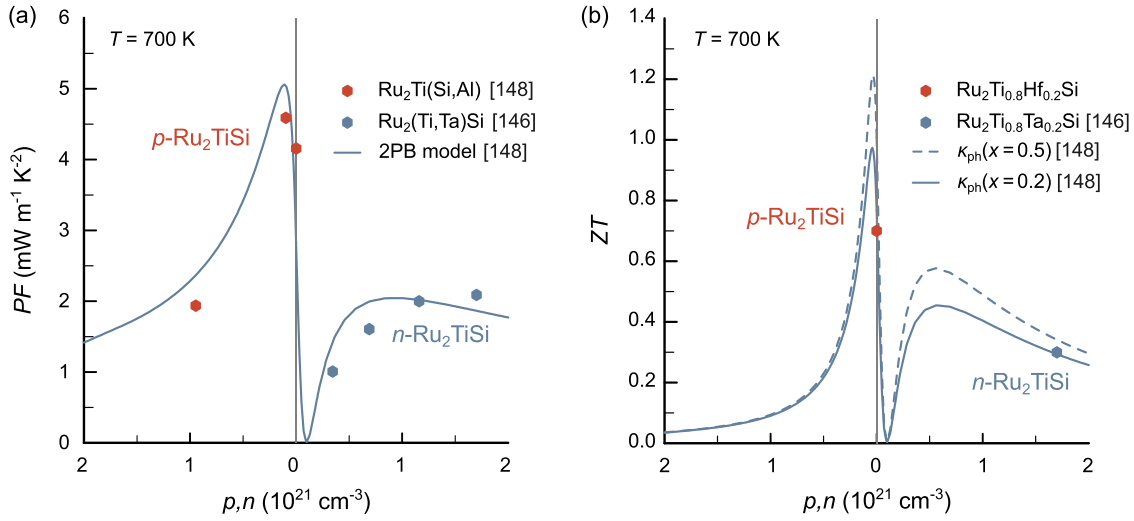

Figure 11. Modeling and thermoelectric performance predictions as a function of doping for Ru_2TiSi-based Heusler compounds. (a) Doping-dependent power factor for *p*- and *n*-type Ru_2TiSi. Solid line represents theoretical curve, calculated from a two-parabolic band model. Red symbols refer to experimental data of *p*-doped $Ru_2TiSi_{1-x}Al_x$ from ref [149]. and blue symbols refer to *n*-doped $Ru_2Ti_{1-x}Ta_xSi$ from ref [147]. (b) Doping-dependent *ZT*. Solid and dashed lines were calculated for different values of the lattice thermal conductivity as discussed in ref [149]. Here, *x* refers to the concentration of heavy 5*d* elements substituted at the Ti site.

(X = Li, K, Ca, Sr, Ba; Y = Cs, Tl, Au, Ag; Z = Sn, Pb, As, Sb, Bi) with intrinsically ultralow thermal conductivities (owing to lattice anharmonicity) and extremely high $ZT = 2 - 5$ [150–153]. These predictions spark excitement but have yet to be confirmed experimentally, as the high cost, chemical reactivity, toxicity, etc., pose challenges for experimental investigations.

7. Conclusion

Summarizing, there has been substantial progress in the development of full-Heusler compounds for thermoelectrics. Fe_2VAl-based systems, discovered more than two decades ago [66,154], are attractive for their low cost, good recyclability and excellent mechanical and chemical long-term stability. While ZT_{max} of these systems has long hovered below 0.2, ZT values larger than 0.3 are no longer an exception, and recent studies with sophisticated nano- and microstructure engineering have even reported ZT values up to 0.4–0.5 around room-temperature, closing in on those of state-of-the-art materials, such as Bi_2Te_3 with $ZT = 0.8 - 1$ at 300 K [128,129]. Apart from enhancements of the figure of merit, there has been huge progress in understanding the electronic structure and how to tune it with respect to thermoelectricity [31,51]. Novel concepts, such as selective localization of charge carriers [36], ultrahigh off-stoichiometry [101,103,108,110] to expand the band gap and induce resonant states or incorporating topological-insulating grain boundary phases to decouple charge and heat transport [127], have been developed and successfully applied. Another interesting direction that has been explored is to enhance the Seebeck coefficient through magnetic spin entropy, which works particularly well for Fe_2VAl-based systems that are close to the magnetic instability and can be easily tuned towards a weakly magnetic state via doping [35,155]. A future challenge will be combining these strategies to optimally enhance both electronic and thermal transport properties. The recent discoveries of Ru_2TiSi-based full-Heusler semiconductors are reviewed and discussed, as well. These materials intrinsically display promising electronic structure features, such as a narrow band gap $E_g = 0.2 - 0.3$ eV, highly dispersive valence band states and a lower thermal conductivity compared to FeVAl-based compounds [147,149]. Multi-carrier transport modeling reveals a high potential figure of merit $ZT > 1$ for Ru_2TiSi-based systems upon proper reduction of the lattice thermal conductivity. Even though the high cost of Ru poses constraints for widespread applications and makes these materials less attractive from an economic point of view compared to their Fe_2VAl relatives, these findings serve as a proof-of-concept that high ZT can be achieved in full-Heusler compounds and motivate a systematic search of other stable full-Heusler phases with semiconducting ground states.

Note

1. Manuscript in preparation, Garmroudi F., Serhiienko I., Parzer M., Pustogow A., Mori T. and Bauer E. (2025).

Disclosure statement

No potential conflict of interest was reported by the author(s).

Funding

Financial support came from the Japan Science and Technology Agency (JST), program MIRAI, Grant No. [JPMJMI19A1].

ORCID

F. Garmroudi http://orcid.org/0000-0002-0088-1755
T. Mori http://orcid.org/0000-0003-2682-1846

References

[1] CRC Handbook of Thermoelectrics. CRC Press; 1995. Available from 10.1201/9781420049718
[2] Thermoelectrics handbook, macro to Nano. CRC Press; 2006. Available from 10.1201/9781420038903
[3] Goldsmid HJ, Douglas RW. The use of semiconductors in thermoelectric refrigeration. Br J Appl Phys. 1954 nov;5(11):386. doi: 10.1088/0508-3443/5/11/303
[4] Goldsmid HJ XXVII. Thermoelectric applications of semiconductors. J Electron Control. 1955;1 (2):218–222. doi: 10.1080/00207215508961410
[5] Birkholz U. Untersuchung der intermetallischen Verbindung Bi2Te3 sowie der festen Lösungen Bi2-xSbxTe3 und Bi2Te3-xSex hinsichtlich ihrer Eignung als Material für Halbleiter-Thermoelemente. Z für Naturforschung A. 1958 Sep;13(9):780–792. doi: 10.1515/zna-1958-0910
[6] Heusler F. Über magnetische manganlegierungen. Verh Dtsch Phys Ges. 1903;5:219.
[7] Harang L. XVI. Über die Kristallstruktur der Heuslerschen Legierungen. Z Kristallog - Crystalline Mater. 1927;65(1–6):261. https://archive.org/details/zeitschrift-fuer-kristallographie-crystalline-materials192765/page/262/mode/2up
[8] Young JFT XXVIII. The crystal structure of various Heusler alloys by the use of X-rays. Lond, Edinburgh Dublin Phil Mag J Sci. 1923;46(272):291–305. doi: 10.1080/14786442308634246
[9] Heusler O. Kristallstruktur und Ferromagnetismus der Mangan-Aluminium-Kupferlegierungen. Annalen der Phys. 1934;411(2):155–201. doi: 10.1002/andp.19344110205
[10] Bradley AJ, Rodgers JW. The crystal structure of the heusler alloys. Proc R Soc Lond A Math Phys Sci. 1934 Mar;144:340–359.

[11] Galanakis I, Dederichs PH, Papanikolaou N. Slater-Pauling behavior and origin of the half-metallicity of the full-Heusler alloys. Phys Rev B. 2002 Nov;66 (17):174429. doi: 10.1103/PhysRevB.66.174429
[12] Slater JC. The ferromagnetism of nickel. II. Temperature effects. Phys Rev. 1936 Jun;49 (12):931–937. doi: 10.1103/PhysRev.49.931
[13] Pauling L. The nature of the interatomic forces in metals. Phys Rev. 1938 Dec;54(11):899–904. https://link.aps.org/doi/10.1103/PhysRev.54.899
[14] Umetsu RY, Kobayashi K, Fujita A, et al. Magnetic properties and stability of L21 and B2 phases in the Co2MnAl Heusler alloy. J Appl Phys. 2008 04;103 (7):07D718. doi: 10.1063/1.2836677
[15] Wurmehl S, Fecher GH, Kandpal HC, et al. Investigation of Co_2FeSi: the Heusler compound with highest Curie temperature and magnetic moment. Appl Phys Lett. 2006 01;88(3):032503. doi: 10.1063/1.2166205
[16] Galanakis I, Özdoğan K, Şaşıoğlu E, et al. Doping of Mn_2VAl and Mn_2VSi Heusler alloys as a route to half-metallic antiferromagnetism. Phys Rev B. 2007 Mar;75(9):092407. https://link.aps.org/doi/10.1103/PhysRevB.75.092407
[17] Graf T, Felser C, Parkin SS. Simple rules for the understanding of Heusler compounds. Prog In Solid State Nat. 2011;39(1):1–50. doi: 10.1016/j.progsolidstchem.2011.02.001
[18] Bhat TM, Gupta DC. Effect of on-site Coulomb interaction on electronic and transport properties of 100. J Magn Magn Mater. 2017;435:173–178. https://www.sciencedirect.com/science/article/pii/S0304885316331201
[19] Gao GY, Hu L, Yao KL, et al. Large half-metallic gaps in the quaternary Heusler alloys CoFeCrZ (Z=al, Si, Ga, Ge): a first-principles study. J Alloys Compd. 2013;551:539–543. doi: 10.1016/j.jallcom.2012.11.077
[20] Pandey B, Ray RB, Kaphle GC. First-principles study of structural, electronic and magnetic properties of Co-based quaternary Heusler compounds: CoFeCrAl, CoFeTiAs, CoFeCrGa and CoMnVAs. BIBECHANA. 2017 Dec;15:50–59. https://www.nepjol.info/index.php/BIBECHANA/article/view/18344
[21] Li GJ, Liu EK, Zhang YJ, et al. Structure, magnetism, and magnetic compensation behavior of Co50-xMn25ga25+x and Co50-xMn25 +xga25 Heusler alloys. J Appl Phys. 2013 03;113 (10):103903. doi: 10.1063/1.4794811
[22] Samanta T, Bhobe PA, Das A, et al. Reentrant cluster glass and stability of ferromagnetism in the Ga_2MnCo Heusler alloy. Phys Rev B. 2018 May;97(18):184421. doi: 10.1103/PhysRevB.97.184421
[23] Barman SR, Chakrabarti A, Singh S, et al. Theoretical prediction and experimental study of a ferromagnetic shape memory alloy: Ga_2MnNi. Phys Rev B. 2008 Oct;78(13):134406. doi: 10.1103/PhysRevB.78.134406
[24] Wang JL, Ma L, Hofmann M, et al. Neutron diffraction study of MnNiGa2—structural and magnetic behaviour. J Appl Phys. 2014 01;115(17):17A904. doi: 10.1063/1.4857455
[25] Faleev SV, Ferrante Y, Jeong J, et al. Origin of the tetragonal ground state of Heusler compounds. Phys Rev Appl. 2017;7(3):034022. doi: 10.1103/PhysRevApplied.7.034022
[26] Mostefa Z, Cherifi F, Boukra A, et al. Martensitic phase transformations in quaternary Heusler alloys Co2Ti1-xFexas. Acta Phys Pol A. 2021 Aug;140 (2):175–180. doi: 10.12693/APhysPolA.140.175
[27] Webster Slt K R A Ziebeck PJ, Peak MS, Town SL. Magnetic order and phase transformation in Ni2MnGa. Phil Mag B. 1984;49(3):295–310. doi. 10.1080/13642817408246515
[28] Keshavarz S, Naghibolashrafi N, Jamer ME, et al. Fe_2MnGe: a hexagonal Heusler analogue. J Alloys Compd. 2019;771:793–802. doi: 10.1016/j.jallcom.2018.07.298
[29] Wederni A, Daza J, Ben Mbarek W, et al. Crystal structure and properties of Heusler Alloys: a comprehensive review. Metals. 2024;14: 6):688. doi: 10.3390/met14060688
[30] Brod MK, Guo S, Zhang Y, et al. Explaining the electronic band structure of half-Heusler thermoelectric semiconductors for engineering high valley degeneracy. MRS Bull. 2022;47(6):573–583. doi: 10.1557/s43577-022-00360-z
[31] Hinterleitner B, Garmroudi F, Reumann N, et al. The electronic pseudo band gap states and electronic transport of the full-Heusler compound Fe_2VAl. J Mater Chem C. 2021;9(6):2073–2085. doi: 10.1039/D0TC05187J
[32] Garmroudi F, Parzer M, Riss A, et al. Pivotal role of carrier scattering for semiconductorlike transport in Fe_2VAl. Phys Rev B. 2023;107(8):L081108. doi: 10.1103/PhysRevB.107.L081108
[33] Bandaru S, Jund P. Electronic structure of the Heusler compound Fe_2VAl and its point defects by ab initio calculations. Physica Status solidi (b). 2017;254 (2):1600441. doi: 10.1002/pssb.201600441
[34] Garmroudi F, Parzer M, Riss A, et al. Anderson transition in stoichiometric Fe_2VAl: high thermoelectric performance from impurity bands. Nat Commun. 2022;13(1):3599. doi: 10.1038/s41467-022-31159-w
[35] Tsujii N, Garmroudi F, Bauer E, et al. Effect of magnetic entropy in the thermoelectric properties of Fe-doped Fe_2VAl full-Heusler alloy. Mater Today Phys. 2024;48:101568. doi: 10.1016/j.mtphys.2024.101568
[36] Garmroudi F, Parzer M, Riss A, et al. Anderson transition: a novel route to high thermoelectric performance. 2021.
[37] Maier S, Denis S, Adam S, et al. Order-disorder transitions in the Fe_2VAl Heusler alloy. Acta Materialia. 2016;121:126–136. doi: 10.1016/j.actamat.2016.08.080
[38] Mahan GD, Sofo JO. The best thermoelectric. Proc Natl Acad Sci USA. 1996;93(15):7436–7439. https://www.pnas.org/doi/abs/10.1073/pnas.93.15.7436
[39] Bilc DI, Hautier G, Waroquiers D, et al. Low-dimensional transport and large thermoelectric power factors in bulk semiconductors by band engineering of highly directional electronic states. Phys Rev Lett. 2015 Mar;114(13):136601. doi: 10.1103/PhysRevLett.114.136601
[40] Garmroudi F, Riss A, Parzer M, et al. Boosting the thermoelectric performance of Fe_2VAl- type Heusler compounds by band engineering. Phys Rev B. 2021;103:085202.
[41] Garmroudi F, Parzer M, Riss A, et al. Large thermoelectric power factors by opening the band gap in semimetallic Heusler alloys. Mater Today Phys. 2022;27:100742. doi: 10.1016/j.mtphys.2022.100742

[42] Nishino Y, Kato M, Asano S, et al. Semiconductorlike behavior of electrical resistivity in Heusler-type Fe_2 VAl compound. Phys Rev Lett. 1997;79(10):1909. doi: 10.1103/PhysRevLett.79.1909
[43] Soda K, Mizutani T, Yoshimoto O, et al. High-resolution photoelectron spectroscopy of Heusler-type Fe_2VAl alloy. J Synchrotron Radiat. 2002;9 (4):233–236. doi: 10.1107/S0909049502009214
[44] Okamura H, Kawahara J, Nanba T, et al. Pseudogap formation in the intermetallic compounds $(Fe_{1-x}V_x)_3Al$. Phys Rev Lett. 2000;84(16):3674. doi: 10.1103/PhysRevLett.84.3674
[45] Lue CS, Ross JH. Semimetallic behavior in Fe2VAl: NMR evidence. Phys Rev B. 1998;58(15):9763. doi: 10.1103/PhysRevB.58.9763
[46] Ooiwa K, Endo K. Nuclear magnetic relaxation in Heusler alloys Fe_2VGa and Fe_2VAl. J Magnetism And Magnetic Mater. 1998;177:1443–1444. doi: 10.1016/S0304-8853(97)00573-8
[47] Weinert M, Watson R. Hybridization-induced band gaps in transition-metal aluminides. Phys Rev B. 1998;58(15):9732. doi: 10.1103/PhysRevB.58.9732
[48] Singh D, Mazin I. Electronic structure, local moments, and transport in Fe_2VAl. Phys Rev B. 1998;57(22):14352. doi: 10.1103/PhysRevB.57.14352
[49] Shastri SS, Pandey SK. A comparative study of different exchange-correlation functionals in understanding structural, electronic and thermoelectric properties of Fe_2VAl and Fe_2TiSn compounds. Comput Mater Sci. 2018;143:316–324. doi: 10.1016/j.commatsci.2017.10.053
[50] Bilc DI, Ghosez P. Electronic and thermoelectric properties of Fe_2VAl: the role of defects and disorder. Phys Rev B. 2011;83(20):205204. doi: 10.1103/PhysRevB.83.205204
[51] Anand S, Gurunathan R, Soldi T. Thermoelectric transport of semiconductor full-Heusler VFe_2Al. J Mater Chem C. 2020;8(30):10174–10184. doi: 10.1039/D0TC02659J
[52] Perdew JP, Burke K, Ernzerhof M. Generalized gradient approximation made simple. Phys Rev Lett. 1996 Oct;77(18):3865–3868. doi: 10.1103/PhysRevLett.77.3865
[53] Engel E, Vosko SH. Exact exchange-only potentials and the virial relation as microscopic criteria for generalized gradient approximations. Phys Rev B. 1993 May;47(20):13164–13174. doi: 10.1103/PhysRevB.47.13164
[54] Tran F, Blaha P. Accurate band gaps of semiconductors and insulators with a semilocal exchange-correlation potential. Phys Rev Lett. 2009 Jun;102(22):226401. doi: 10.1103/PhysRevLett.102.226401
[55] Anisimov VI, Aryasetiawan F, Lichtenstein A. First-principles calculations of the electronic structure and spectra of strongly correlated systems: the LDA+ U method. J Phys Condens Matter. 1997;9(4):767. doi: 10.1088/0953-8984/9/4/002
[56] Adamo C, Barone V. Toward reliable density functional methods without adjustable parameters: the PBE0 model. J. Chem. Phys. 1999;110(13):6158–6170. doi: 10.1063/1.478522
[57] Bilc DI, Orlando R, Shaltaf R, et al. Hybrid exchange correlation functional for accurate prediction of the electronic and structural properties of ferroelectric oxides. Phys Rev B. 2008 Apr;77 (16):165107. https://link.aps.org/doi/10.1103/PhysRevB.77.165107
[58] Tomczak JM. Thermoelectricity in correlated narrow-gap semiconductors. J Phys Condens Matter. 2018;30(18):183001. doi: 10.1088/1361-648X/aab284
[59] Garmroudi F, Parzer M, Riss A, et al. Solubility limit and annealing effects on the microstructure & thermoelectric properties of Fe2V1–xTax Al1–ySiy Heusler compounds. Acta Materialia. 2021;212:116867. doi: 10.1016/j.actamat.2021.116867
[60] Lee HW, Hsing CR, Chang CM, et al. Electronic structures of 24-valence-electron full Heusler compounds investigated by density functional and GW calculations. J Phys Condens Matter. 2020;32 (17):175501. doi: 10.1088/1361-648X/ab6a30
[61] Lue C, Ross JH Jr, Chang C, et al. Field-dependent specific heat in Fe_2VAl and the question of possible 3d heavy fermion behavior. Phys Rev B. 1999;60(20): R13941. doi: 10.1103/PhysRevB.60.R13941
[62] Nishino Y, Tamada Y. Doping effects on thermoelectric properties of the off-stoichiometric Heusler compounds $Fe_{2-x}V_{1+x}$ Al. J Appl Phys. 2014;115 (12):123707. doi: 10.1063/1.4869395
[63] Nishino Y. Development of thermoelectric materials based on Fe_2VAl Heusler compound for energy harvesting applications. IOP Conf Ser Mater Sci Eng. 2011;18(14):142001. doi: 10.1088/1757-899X/18/14/142001
[64] Nishino Y, Deguchi S, Mizutani U. Thermal and transport properties of the Heusler-type $Fe_2VAl_{1-x}Ge_x$ ($0 \le x \le 0.20$) alloys: effect of doping on lattice thermal conductivity, electrical resistivity, and Seebeck coefficient. Phys Rev B. 2006;74(11):115115. doi: 10.1103/PhysRevB.74.115115
[65] Garmroudi F, Parzer M, Riss A, et al. Solubility limit and annealing effects on the microstructure & thermoelectric properties of $Fe_2V_{1-x}Ta_x$ $Al_{1-y}Si_y$ Heusler compounds. Available at SSRN 3762208.
[66] Kato H, Kato M, Nishino Y, et al. Effect of silicon substitution on thermoelectric properties of Heusler-type Fe_2VAl alloy. Nippon Kinzoku Gakkaishi (1952). 2001;65(7):652–656. doi: 10.2320/jinstmet1952.65.7_652
[67] Hinterleitner B, Fuchs P, Rehak J, et al. Stoichiometric and off-stoichiometric full Heusler $Fe_2V_{1-x}W_x$ Al thermoelectric systems. Phys Rev B. 2020;102 (7):075117. doi: 10.1103/PhysRevB.102.075117
[68] Renard K, Mori A, Yamada Y, et al. Thermoelectric properties of the Heusler-type Fe_2VTa_x Al_{1-x} alloys. J Appl Phys. 2014;115(3):033707. doi: 10.1063/1.4861419
[69] Vasundhara M, Srinivas V, Rao V. Electronic transport in Heusler-type $Fe_2VAl_{1-x}M_x$ alloys (M= B, in, Si). Phys Rev B. 2008;77(22):224415. doi: 10.1103/PhysRevB.77.224415
[70] Vasundhara M, Srinivas V, Rao V. Low-temperature electrical transport in Heusler-type $Fe_2V(AlSi)$ alloys. J Phys Condens Matter. 2005;17(38):6025. doi: 10.1088/0953-8984/17/38/008
[71] Lue CS, Chen C, Lin J, et al. Thermoelectric properties of quaternary Heusler alloys Fe_2VAl_{1-x} Si_x. Phys Rev B. 2007;75(6):064204. doi: 10.1103/PhysRevB.75.064204
[72] Mikami M, Ozaki K, Takazawa H, et al. Effect of Ti substitution on thermoelectric properties of W-doped Heusler Fe_2VAl alloy. J Elec Materi. 2013;42 (7):1801–1806. doi: 10.1007/s11664-012-2433-7

[73] Nakayama H, Ide N, Nishino Y. Thermoelectric properties of P-Type Heusler compounds ($Fe_{2-x}Co_x$)($V_{1-y}Ti_y$)Al. Mater Trans. 2008;49 (8):1858–1862. doi: 10.2320/matertrans.MRA2008078

[74] Terazawa Y, Mikami M, Itoh T, et al. Effects of heavy element substitution on electronic structure and lattice thermal conductivity of Fe_2VAl thermoelectric material. J Elec Materi. 2012;41(6):1348–1353. doi: 10.1007/s11664-011-1862-z

[75] Sandaiji Y, Ide N, Nishino Y, et al. Off-stoichiometric effects on thermoelectric properties of Fe_2VAl-based compounds. J Jpn Soc Powder Powder Metall. 2010;57(4):207–212. doi: 10.2497/jjspm.57.207

[76] Lu W, Zhang W, Chen L. Thermoelectric properties of $(Fe_{1-x}Co_x)_2VAl$ Heusler-type compounds. J Alloys And Compd. 2009;484(1–2):812–815. doi: 10.1016/j.jallcom.2009.05.032

[77] Reumann N, Riss A, Garmroudi F, et al. Thermoelectric properties and low-temperature transport anomalies in the p-type full-Heusler compounds $Fe_{2-x}Cr_xVAl$. Phys Rev B. 2022;106 (23):235138. doi: 10.1103/PhysRevB.106.235138

[78] Hsu KF, Loo S, Guo F, et al. Cubic $AgPb_mSbTe_{2+m}$: bulk thermoelectric materials with high figure of merit. Science. 2004;303(5659):818–821. doi: 10.1126/science.1092963

[79] Weht R, Pickett W. Excitonic correlations in the intermetallic Fe_2VAl. Phys Rev B. 1998;58(11):6855. doi: 10.1103/PhysRevB.58.6855

[80] Venkatesh C, Srinivas V, Rao V, et al. Effect of site disorder on the electronic properties of Fe_2VAl Heusler alloy. J Alloys And Compd. 2013;577:417–425. doi: 10.1016/j.jallcom.2013.05.175

[81] Berche A, Noutack MT, Doublet ML, et al. Unexpected band gap increase in the Fe_2VAl Heusler compound. Mater Today Phys. 2020;13:100203. doi: 10.1016/j.mtphys.2020.100203

[82] Kristanovski O, Richter R, Krivenko I, et al. Quantum many-body intermetallics: phase stability of Fe $_3$ Al and small-gap formation in Fe 2 VAl. Phys Rev B. 2017;95(4):045114. doi: 10.1103/PhysRevB.95.045114

[83] Miyazaki H, Tanaka S, Ide N, et al. Thermoelectric properties of Heusler-type off-stoichiometric $Fe_2V_{1+x}Al_{1-x}$ alloys. Mater Res Express. 2013;1(1):015901. doi: 10.1088/2053-1591/1/1/015901

[84] Liu W, Zhou J, Jie Q, et al. New insight into the material parameter B to understand the enhanced thermoelectric performance of $Mg_2Sn_{1-x-y}Ge_xSb_y$. Energy Environ Sci. 2016;9(2):530–539. doi: 10.1039/C5EE02600H

[85] Androulakis J, Todorov I, He J, et al. Thermoelectrics from abundant chemical elements: high-performance nanostructured PbSe–PbS. J Am Chem Soc. 2011;133 (28):10920–10927. doi: 10.1021/ja203022c

[86] LaLonde AD, Pei Y, Snyder GJ. Reevaluation of $PbTe_{1-x}I_x$ as high performance n-type thermoelectric material. Energy Environ Sci. 2011;4(6):2090–2096. doi: 10.1039/c1ee01314a

[87] Liu W, Tan X, Yin K, et al. Convergence of conduction bands as a means of enhancing thermoelectric performance!? format?. Of n-type $Mg_2Si1_{-x}Sn_x$ solid solutions. Phys Rev Lett. 2012;108(16):166601. doi: 10.1103/PhysRevLett.108.166601

[88] Cha J, Zhou C, Cho SP, et al. Ultrahigh power factor and electron mobility in n-type Bi_2Te_3–x% Cu stabilized under excess Te condition. ACS Appl Mater Interfaces. 2019;11(34):30999–31008. doi: 10.1021/acsami.9b10394

[89] Jha R, Tsujii N, Garmroudi F, et al. Unexpected p-type thermoelectric transport arising from magnetic Mn substitution in Fe2V1–xMnx Al Heusler compounds. J Mater Chem C. 2024;12 (24):8861–8872. doi: 10.1039/D4TC00779D

[90] Rowe D, Kuznetsov V, Kuznetsova L, et al. Electrical and thermal transport properties of intermediate-valence $YbAl_3$. J Phys D Appl Phys. 2002;35(17):2183. doi: 10.1088/0022-3727/35/17/315

[91] Garmroudi F, Parzer M, Riss A, et al. High thermoelectric performance in metallic NiAu alloys via interband scattering. Sci Adv. 2023;9(37):eadj1611. doi: 10.1126/sciadv.adj1611

[92] Lue CS, Kuo YK. Thermoelectric properties of the semimetallic Heusler compounds $Fe_{2-x}V_{1+x}$ M (M= Al, Ga). Phys Rev B. 2002;66(8):085121. doi: 10.1103/PhysRevB.66.085121

[93] Naka T, Sato K, Taguchi M, et al. Ferromagnetic quantum singularities and small pseudogap formation in Heusler type $Fe_{2+x}V_{1-x}$ Al. Phys Rev B. 2012;85(8):085130. doi: 10.1103/PhysRevB.85.085130

[94] Soda K, Harada S, Hayashi T, et al. Angle-resolved photoemission analysis of electronic structures for thermoelectric properties of off-stoichiometric $Fe_{2-x}V_{1+x}Al$ alloys. Mater Trans. 2016;57(7):1040–1044. doi: 10.2320/matertrans.MF201603

[95] Naka T, Nikitin AM, Pan Y, et al. Composition induced metal–insulator quantum phase transition in the Heusler type Fe_2 VAl. J Phys Condens Matter. 2016;28(28):285601. doi: 10.1088/0953-8984/28/28/285601

[96] Diack-Rasselio A, Rouleau O, Coulomb L, et al. Influence of self-substitution on the thermoelectric Fe_2VAl Heusler alloy. J Alloys And Compd. 2022;920:166037. doi: 10.1016/j.jallcom.2022.166037

[97] Takagiwa Y, Iwasaki Y. Effect of off-stoichiometry and point defects on thermoelectric properties of a W-Substituted Fe_2VAl Heusler compound. ACS Appl Energy Mater. 2023;6(15):8256–8265. doi: 10.1021/acsaem.3c01370

[98] Soda K, Harada S, Kato M, et al. Origin of large thermoelectric power in off-stoichiometric Fe_2VAl-based alloys. In: IOP Conference Series: Materials Science and Engineering, ICC3: Symposium 9C: Ceramics for Electricity held in Osaka, Japan. IOP Publishing; 2011. Vol. 18. p. 142004.

[99] Takeuchi T, Terazawa Y, Furuta Y, et al. Effect of heavy element substitution and off-stoichiometric composition on thermoelectric properties of Fe_2VAl-Based Heusler phase. J Elec Materi. 2013;42 (7):2084–2090. doi: 10.1007/s11664-013-2532-0

[100] Mikami M, Inukai M, Miyazaki H, et al. Effect of off-stoichiometry on the thermoelectric properties of Heusler-type Fe 2 VAl sintered alloys. J Elec Materi. 2016;45(3):1284–1289. doi: 10.1007/s11664-015-3999-7

[101] Nishino Y, Kamizono S, Miyazaki H, et al. Effects of off-stoichiometry and Ti doping on thermoelectric performance of Fe_2VAl Heusler compound. AIP Adv. 2019;9(12). doi: 10.1063/1.5123783

[102] Alleno E, Diack-Rasselio A, Noutack MT, et al. Optimization of the thermoelectric properties in

self-substituted Fe_2VAl. Phys Rev Mater. 2023;7 (7):075403. doi: 10.1103/PhysRevMaterials.7.075403
[103] Asai M, Miyazaki H, Nishino Y. Tailoring p-type thermoelectric properties of the Fe_2Val Heusler compound through off-stoichiometry and multiple substitution. J Alloys And Compd. 2025;1013:178643. doi: 10.1016/j.jallcom.2025.178643
[104] Soda K, Osawa S, Kato M, et al. Semiconducting transport properties in off-stoichiometric $Fe_{2-x}VAl_{1+x}$. In: Proceedings of the International Conference on Strongly Correlated Electron Systems (SCES2013); Tokyo, Japan; 2014. p. 017036.
[105] Nishino Y, Kato H, Kato M, et al. Effect of off-stoichiometry on the transport properties of the Heusler-type Fe_2VAl compound. Phys Rev B. 2001;63(23):233303. doi: 10.1103/PhysRevB.63.233303
[106] Sato K, Naka T, Taguchi M, et al. Weak itinerant ferromagnetism in Heusler-type $Fe_2VAl_{0.95}$. Phys Rev B. 2010;82(10):104408. doi: 10.1103/PhysRevB.82.104408
[107] Van der Rest C, Schmitz A, Jacques PJ. On the characterisation of antisite defects and ordering in off-stoichiometric Fe_2VAl-based Heusler compounds by X-ray anomalous diffraction. Acta Materialia. 2018;142:193–200. doi: 10.1016/j.actamat.2017.09.024
[108] Parzer M, Garmroudi F, Riss A, et al. High solubility of Al and enhanced thermoelectric performance due to resonant states in Fe_2VAlx. Appl Phys Lett. 2022;120(7):120. doi: 10.1063/5.0077159
[109] Ślebarski A, Fija Lkowski M, Deniszczyk J, et al. Off-stoichiometriceffect on magnetic and electron transport properties of Fe 2 VAl 1.35 and Ni 2 VAl: a comparative study. Phys Rev B. 2024;109 (16):165105. doi: 10.1103/PhysRevB.109.165105
[110] Parzer M, Garmroudi F, Riss A, et al. Semiconducting Heusler compounds beyond the Slater-Pauling rule. PRX Energy. 2024;3(3):033006. doi: 10.1103/PRXEnergy.3.033006
[111] Parzer M, Garmroudi F, Riss A, et al. Mapping delocalization of impurity bands across archetypal mott-Anderson transition. Physical Review Letters. 2025;135:066302.
[112] Parzer M. Extending the phase space of full-Heusler compounds for thermoelectrics. TU Wien; 2024.
[113] *Enhanced thermopower by double-site substitution of Ti in Fe2(VAl)1–x Ti2x*, *author= Parzer*, *M* and Kositz, *A* and *Süs*, *J* and *Garmroudi*, *F* and *Mori*, *T* and *Bauer*, *E*, journal=materials Today Physics, pages=101712. 2025, *p*ublisher=Elsevier.
[114] Parzer M, Riss A, Garmroudi F, et al. SeeBand: a highly efficient, interactive tool for analyzing electronic transport data. arXiv preprint arXiv:240906261 Npj Comput Mater. 2024;11(1). doi: 10.1038/s41524-025-01645-y
[115] Garmroudi F, Parzer M, Knopf M, et al. Unveiling the structure-property relationship in metastable Heusler compounds by systematic disorder tuning. Phys Rev B. 2023;107(1):014108. doi: 10.1103/PhysRevB.107.014108
[116] Alleno E, Berche A, Crivello JC, et al. On the structure and electronic properties of $Fe_2V_{0.8}W_{0.2}Al$ thin films. Phys Chem Chem Phys. 2020;22(39):22549–22554. doi: 10.1039/D0CP03738A
[117] Kobayashi F, Ide N, Nishino Y. Effects of Re substitution on thermoelectric properties of pseudogap System Fe_2VAl. J Jpn Inst Met. 2007;71(2):208–212. doi: 10.2320/jinstmet.71.208
[118] Group TSEP, Kurosaki K, Muta H, et al. Effect of Nb substitution for V on the thermoelectric properties of Fe_2VAl. J Alloys And Compd. 2009;486(1–2):507–-510. doi: 10.1016/j.jallcom.2009.06.202
[119] Sugiura T, Nishino Y. Doping effects of transition metals on thermoelectric properties of off-stoichiometric Fe_2VAl alloys. J Jpn Inst Met. 2009;73(11):846–851. doi: 10.2320/jinstmet.73.846
[120] Mikami M, Kinemuchi Y, Ozaki K, et al. Thermoelectric properties of tungsten-substituted Heusler Fe_2VAl alloy. J Appl Phys. 2012;111(9):111. doi: 10.1063/1.4710990
[121] Knapp I, Budinska B, Milosavljevic D, et al. Impurity band effects on transport and thermoelectric properties of $Fe_{2-x}Ni_xVAl$. Phys Rev B. 2017;96(4):045204. doi: 10.1103/PhysRevB.96.045204
[122] Garmroudi F, Parzer M, Riss A, et al. Solubility limit and annealing effects on the microstructure and thermoelectric properties of $Fe_2V_{1-x}Ta_x Al_{1-y} Si_y$ Heusler compounds. Acta Materialia. 2021;212:116867. submitted 17/12/2020.
[123] Rogl G, Grytsiv A, Rogl P, et al. N-type skutterudites (R, Ba, Yb)yCo4Sb12 (R = Sr, La, mm, DD, SrMm, SrDD) approaching ZT ≈ 2.0. Acta Materialia. 2014;63(63):30–43. doi: 10.1016/j.actamat.2013.09.039
[124] Do D, Lee MS, Mahanti SD. Effect of onsite Coulomb repulsion on thermoelectric properties of full-Heusler compounds with pseudogaps. Phys Rev B. 2011;84 (12):125104. doi: 10.1103/PhysRevB.84.125104
[125] Mikami M, Matsumoto A, Kobayashi K. Synthesis and thermoelectric properties of microstructural Heusler Fe_2VAl alloy. J Alloys And Compd. 2008;461(1–2):423–426. doi: 10.1016/j.jallcom.2007.07.004
[126] Yabuuchi S, Okamoto M, Nishide A, et al. Large Seebeck coefficients of Fe_2TiSn and Fe_2TiSi: first-principles study. Appl Phys Express. 2013;6 (2):025504. doi: 10.7567/APEX.6.025504
[127] Bergman DJ, Levy O. Thermoelectric properties of a composite medium. J Appl Phys. 1991;70 (11):6821–6833. doi: 10.1063/1.349830
[128] Mao J, Zhu H, Ding Z, et al. High thermoelectric cooling performance of n-type Mg_3Bi_2-based materials. Science. 2019;365(6452):495–498. doi: 10.1126/science.aax7792
[129] Tsujii N, Nishide A, Hayakawa J, et al. Observation of enhanced thermopower due to spin fluctuation in weak itinerant ferromagnet. Sci Adv. 2019;5(2): eaat5935. doi: 10.1126/sciadv.aat5935
[130] Mikami M, Tanaka S, Kobayashi K. Thermoelectric properties of Sb-doped Heusler Fe_2VAl alloy. J Alloys And Compd. 2009;484(1–2):444–448. doi: 10.1016/j.jallcom.2009.04.120
[131] Masuda S, Tsuchiya K, Qiang J, et al. Effect of high-pressure tor- sion on the microstructure and thermoelectric properties of Fe2VAl-based compounds. J Appl Phys. 2018;124(3):035106. doi: 10.1063/1.5034390
[132] Fukuta K, Tsuchiya K, Miyazaki H, et al. Improving thermoelectric performance of Fe2VAl-based Heusler compounds via high-pressure torsion. Appl Phys A. 2022;128(3):184. doi: 10.1007/s00339-022-05329-y
[133] Rogl G, Rogl PF. High pressure torsion, a large-scale manufacturing tool for high ZT skutterudite

thermoelectrics. Z für Anorg und Allg Chem. 2022;648(15):e202200044. doi: 10.1002/zaac.202200044

[134] Rogl G, Garmroudi F, Riss A, et al. Understanding thermal and electronic transport in high-performance thermoelectric skutterudites. Intermetallics. 2022;146:107567. doi: 10.1016/j.intermet.2022.107567

[135] Rogl G, Ghosh S, Wang L, et al. Half-Heusler alloys: enhancement of ZT after severe plastic deformation (ultra-low thermal conductivity). Acta Materialia. 2020;183:285–300. doi: 10.1016/j.actamat.2019.11.010

[136] Garmroudi F, Serhiienko I, Parzer M, et al. Decoupled charge and heat transport in Fe_2VAl composite thermoelectrics with topological-insulating grain boundary networks. Nat Commun. 2025;16(1):2976. doi: 10.1038/s41467-025-57250-6

[137] Riss A, Stöger M, Parzer M, et al. Criteria for erroneous substrate contribution to the thermoelectric performance of thin films. Phys Rev Appl. 2023;19(5):054024. doi: 10.1103/PhysRevApplied.19.054024

[138] Riss A, Garmroudi F, Parzer M, et al. Thermoelectric power factor of composites. Phys Rev Appl. 2024;21(1):014002. doi: 10.1103/PhysRevApplied.21.014002

[139] Snyder GJ, Snyder AH, Wood M, et al. Weighted mobility. Adv Mater. 2020;32(25):2001537. doi: 10.1002/adma.202001537

[140] Ye X, Yu J, Ke S, et al. Excellent thermoelectric performance of Fe_2NbAl alloy induced by strong crystal anharmonicity and high band degeneracy. Npj Quantum Mater. 2024;9(1):60. doi: 10.1038/s41535-024-00671-1

[141] Khandy SA, Islam I, Gupta DC, et al. A case study of Fe_2TaZ (Z=al, Ga, In) Heusler alloys: hunt for half-metallic behavior and thermoelectricity. RSC Adv. 2018;8(71):40996–41002. doi: 10.1039/C8RA04433C

[142] Riss A, Lasisch E, Podbelsek S, et al. Iterative composition optimization in Fe $_2$ VA 1 –based thin-film thermoelectrics using single-target sputtering. Phys Rev Mater. 2024;8(9):095402. doi: 10.1103/PhysRevMaterials.8.095402

[143] Meinert M, Geisler MP, Schmalhorst J, et al. Experimental realization of a semiconducting full-Heusler compound: Fe_2TiSi. Phys Rev B. 2014;90(8):085127. doi: 10.1103/PhysRevB.90.085127

[144] Shimanuki Y, Kudo K, Ishibe T, et al. Thermoelectric properties of single-phase full-Heusler alloy Fe_2TiSi films with D 3-type disordering. J Appl Phys. 2020;127(5):127. doi: 10.1063/1.5141949

[145] Kurosaki Y, Yabuuchi S, Nishide A, et al. Thermoelectric properties of composition-controlled Fe_2TiSi-based full-Heusler thin films. Appl Phys Express. 2022;15(8):085502. doi: 10.35848/1882-0786/ac7e1c

[146] Fujimoto T, Mikami M, Miyazaki H, et al. Enhanced thermoelectric performance of Ru_2TiSi Heusler compounds with Ta substitution. J Alloys And Compd. 2023;969:172345. doi: 10.1016/j.jallcom.2023.172345

[147] Jain A, Ong SP, Hautier G, et al. Commentary: the materials project: a materials genome approach to accelerating materials innovation. APL Mater. 2013;1(1):1. doi: 10.1063/1.4812323

[148] Garmroudi F, Parzer M, Mori T, et al. Thermoelectric transport in Ru2TiSi full-Heusler compounds. PRX Energy. 2025;4: 013010. doi:10.1103/PRXEnergy.4.013010

[149] He J, Amsler M, Xia Y, et al. Ultralow thermal conductivity in full Heusler semiconductors. Phys Rev Lett. 2016;117(4):046602. doi: 10.1103/PhysRevLett.117.046602

[150] Wang SF, Zhang ZG, Wang BT, et al. Intrinsic ultralow lattice thermal conductivity in the full-Heusler compound Ba_2AgSb. Phys Rev Appl. 2022;17(3):034023. doi: 10.1103/PhysRevApplied.17.034023

[151] She A, Sun Y, Zhao Y, et al. Transport and thermoelectric properties of strongly anharmonic full-heusler compounds CsK_2M (m=as, Bi). Mater Today Commun. 2023;34:105134. doi: 10.1016/j.mtcomm.2022.105134

[152] Guo S, Yue J, Li J, et al. Novel room-temperature full-Heusler thermoelectric material Li_2TlSb. Phys Chem Chem Phys. 2024;26(8):6774–6781. doi: 10.1039/D3CP05612K

[153] Nishino Y. Electronic structure and transport properties of pseudogap system Fe_2VAl. Mater Trans. 2001;42(6):902–910. doi: 10.2320/matertrans.42.902

[154] Witting IT, Chasapis TC, Ricci F, et al. The thermoelectric properties of bismuth telluride. Adv Elect Mater. 2019;5(6):1800904. doi: 10.1002/aelm.201800904

[155] Skoug EJ, Zhou C, Pei Y, et al. High thermoelectric power factor near room temperature in full-Heusler alloys. J Elec Materi. 2009;38(7):1221–1223. doi: 10.1007/s11664-008-0626-x